Europäisches Patentamt
Eur pean Patent Office
Office eur péen des brevets

EP00/03890

REC'D 16 JUN 2000
WIPO PCT

4

Bescheinigung Certificate Attestation

Die angehefteten Unterlagen stimmen mit der ursprünglich eingereichten Fassung der auf dem nächsten Blatt bezeichneten europäischen Patentanmeldung überein.

The attached documents are exact copies of the European patent application described on the following page, as originally filed.

Les documents fixés à cette attestation sont conformes à la version initialement déposée de la demande de brevet européen spécifiée à la page suivante.

Patentanmeldung Nr. Patent application No. Demande de brevet n°

99125745.2

PRIORITY DOCUMENT
SUBMITTED OR TRANSMITTED IN COMPLIANCE WITH RULE 17.1(a) OR (b)

Der Präsident des Europäischen Patentamts;
Im Auftrag

For the President of the European Patent Office

Le Président de l'Office européen des brevets
p.o.

I.L.C. HATTEN-HECKMAN

DEN HAAG, DEN
THE HAGUE, 31/05/00
LA HAYE, LE

Europäisches Patentamt | European Patent Office | Office européen des brevets

Blatt 2 der Bescheinigung
Sheet 2 of the certificate
Page 2 de l'attestation

Anmeldung Nr.:
Application no.: 99125745.2
Demande n°:

Anmeldetag:
Date of filing: 23/12/99
Date de dépôt:

Anmelder:
Applicant(s):
Demandeur(s):
Evotec BioSystems GmbH
22525 Hamburg
GERMANY

Bezeichnung der Erfindung:
Title of the invention:
Titre de l'invention:
A method of characterizing fluorescent molecules or other particles using generating functions

In Anspruch genommene Priorität(en) / Priority(ies) claimed / Priorité(s) revendiquée(s)

Staat: State: Pays:	Tag: Date: Date:	Aktenzeichen: File no. Numéro de dépôt:

Internationale Patentklassifikation:
International Patent classification:
Classification internationale des brevets:
/

Am Anmeldetag benannte Vertragstaaten:
Contracting states designated at date of filing: AT/BE/CH/CY/DE/DK/ES/FI/FR/GB/GR/IE/IT/LI/LU/MC/NL/PT/SE
Etats contractants désignés lors du depôt:

Bemerkungen:
Remarks:
Remarques:

A method of characterizing fluorescent molecules or other particles using generating functions

This invention relates to the field of fluorescence spectroscopy, and more particularly to a method for determining characteristic physical quantities of fluorescent molecules or other particles present in a sample.

The primary data of an experiment in fluorescence correlation spectroscopy (FCS) is a sequence of photon counts detected from a microscopic measurement volume. An essential attribute of the fluorescence correlation analysis is the calculation of the second order autocorrelation function of photon detection. This is a way how a stochastic function (of photon counts) is transformed into a statistical function having an expected shape, serving as a means to estimate some parameters of the sample. However, the calculation of the autocorrelation function is not the only way for extracting information about the sample from the sequence of photon counts. Further approaches are based on moment analysis and analysis of the distribution of the number of photon counts per given time interval (Qian and Elson, Proc. Natl. Acad. Sci. USA, 87: 5479 - 483, 1990; Qian and Elson, Biophys. J. 57: 375 - 380, 1990).

The intensity of fluorescence detected from a particle within a sample is not uniform but depends on the coordinates of the particle with respect to the focus of the optical system. Therefore, a reliable interpretation of measurements should account for the geometry of the illuminated measurement volume. Even though the calculation of a theoretical distribution of the number of photon counts is more complex for a bell-shaped profile than for a rectangular one, the distribution of the number of photon counts sensitively depends on values of the concentration and the specific brightness of fluorescent species, and therefore, the measured distributions of the number of photon counts can be used for sample analysis. The term „specific brightness" denotes the mean count rate of the detector from light emitted by a particle of given species situated in a certain point in the sample, conventionally in the point where the value of the spatial brightness profile function is unity.

The first realization of this kind of analysis was demonstrated on the basis of moments of the photon count number distribution (Qian and Elson, Proc. Natl. Acad. Sci. USA, 87: 5479 -

483, 1990). The k-th factorial moment of the photon count number distribution $P(n)$ is defined as

$$F_k = \sum_n \frac{n!}{(n-k)!} P(n). \tag{1}$$

In turn, factorial moments are closely related to factorial cumulants,

$$F_k = \sum_{l=0}^{k-1} C_l^{k-1} K_{k-l} F_l, \tag{2}$$

or

$$K_k = F_k - \sum_{l=1}^{k-1} C_l^{k-1} K_{k-l} F_l. \tag{3}$$

(C_l^k s are binomial coefficients, and K_ks are cumulants.) The basic expression used in moment analysis, derived for ideal solutions, relate k-th order cumulant to concentrations (c_i) and specific brightness values (q_i)

$$K_k = \chi_k \sum_i c_i (q_i T)^k. \tag{4}$$

Here, χ_k is the k-th moment of the relative spatial brightness profile $B(\mathbf{r})$:

$$\chi_k = \int_{(V)} B^k(\mathbf{r}) dV. \tag{5}$$

Usually in FCS, the unit of volume and the unit of B are selected which yield $\chi_1 = \chi_2 = 1$. After selecting this convention, concentrations in the equations are dimensionless, expressing the mean number of particles per measurement volume, and the specific brightness of any species equals the mean count rate from a particle if situated in the focus divided by the numeric value of $B(0)$. The value of this constant is a characteristic of optical equipment. It can be calculated from estimated parameters of the spatial intensity profile (see below). Qian

and Elson used experimental values of the first three cumulants to determine unknown parameters of the sample. The number of cumulants which can be reliably determined from experiments is usually three to four. This sets a limit to the applicability of the moment analysis.

The idea behind the so-called fluorescence intensity distribution analysis (FIDA), which has in detail been described in the international patent application PCT/EP 97/05619 (international publication number WO 98/16814), can be well understood by imagining an ideal case when a measurement volume is uniformly illuminated and when there is almost never more than a single particle illuminated at a time, similar to the ideal situation in cell sorters. Under these circumstances, each time when a particle enters the measurement volume, fluorescence intensity jumps to a value corresponding to the brightness of a given type of particles. Naturally, the probability that this intensity occurs at an arbitrary time moment equals the product of the concentration of a given species and the size of the measurement volume. Another fluorescent species which may be present in the sample solution produces intensity jumps to another value characteristic of this other species. In summary, the distribution of light intensity is in a straightforward way determined by the values of concentration and specific brightness of each fluorescent species in the sample solution.

It is assumed that the light intensity reaching the detector from a particle as a function of coordinates of the particle is constant over the whole measurement volume, and zero outside it. Also, it is assumed that the diffusion of a fluorescent particle is negligible during the counting interval T. In this case, the distribution of the number of photon counts emitted by a single fluorescent species can be analytically expressed as double Poissonian: the distribution of the number of particles of given species within this volume is Poissonian, and the conditional probability of the number of detected photons corresponding to a given number of particles is also Poissonian. The double Poissonian distribution has two parameters: the mean number of particles in the measurement volume, c and the mean number of photons emitted by a single particle per dwell time, qT. The distribution of the number of photon counts n corresponding to a single species is expressed as

$$P(n;c,q) = \sum_{m=0}^{\infty} \frac{c^m}{m!} e^{-c} \frac{(mqT)^n}{n!} e^{-mqT}, \qquad (6)$$

where m runs over the number of molecules in the measurement volume. If $P_i(n)$ denotes the distribution of the number of photon counts from species i, then the resultant distribution $P(n)$ is expressed as

$$P(n) = \sum_{\{n_i\}} \prod_i P_i(n_i)\delta(n, \sum_i n_i) \qquad (7)$$

This means that $P(n)$ can be calculated as a convolution of the series of distributions $P_i(n)$.

Like in FCS, the rectangular sample profile is a theoretical model which can hardly be applied in experiments. One may divide the measurement volume into a great number of volume elements and assume that within each of them, the intensity of a molecule is constant. Contribution to photon count number distribution from a volume element is therefore double Poissonian with parameters cdV and $qTB(\mathbf{r})$. (Here q denotes count rate from a molecule in a selected standard position where $B = 1$, and $B(\mathbf{r})$ is the spatial brightness profile function of coordinates.) The overall distribution of the number of photon counts can be expressed as a convolution integral over double Poissonian distributions. Integration is a one-dimensional rather than a three-dimensional problem here, because the result of integration does not depend on actual positions of volume elements in respect to each other. Figuratively, one may rearrange the three-dimensional array of volume elements into a one-dimensional array, for example in the decreasing order of the value of B.

In a number of first experiments described in the international patent application PCT/EP 97/05619, the photon count number distribution was indeed fitted, using the convolution technique. The sample model consisted of twenty spatial sections, each characterized by its volume V_j and brightness B_j. However, the technique described in this patent application is slow and inconvenient in cases involving a high number of samples to be analyzed, like in diagnostics or drug discovery, or in analyzing distribution functions involving more than a single argument.

Therefore, it is an object of the present invention to present a convenient and much faster technique for analyzing fluorescence intensity fluctuations.

According to the present invention there is provided a method for characterizing fluorescent molecules or other particles in samples, the method comprising the steps of:

a) monitoring fluctuating intensity of fluorescence emitted by the molecules or other particles in at least one measurement volume of a non-uniform spatial brightness profile by measuring numbers of photon counts in primary time intervals by a single or more photon detectors,

b) determining at least one distribution function of numbers of photon counts, $\vec{P}(\mathbf{n})$, from the measured numbers of photon counts,

c) determining physical quantities characteristic to said particles by fitting the experimentally determined distribution function of numbers of photon counts, wherein the fitting procedure involves calculation of a theoretical distribution function of the number of photon counts $P(\mathbf{n})$ through its generating function, defined as $G(\vec{\xi}) = \sum_{\mathbf{n}} \vec{\xi}^{\mathbf{n}} P(\mathbf{n})$.

The formal definition of the generating function of a distribution $P(n)$ is as follows:

$$G(\xi) = \sum_{n=0}^{\infty} \xi^n P(n). \qquad (8)$$

What makes the generating function attractive in count number distribution analysis is the additivity of its logarithm: logarithms of generating functions of photon count number distributions of independent sources, like different volume elements as well as different species, are simply added for the calculation of the generating function of the combined distribution because the transformation (8) maps distribution convolutions into the products of the corresponding generating functions.

In a particular preferred embodiment, one might monitor the fluctuating fluorescence intensity in consecutive primary time intervals of equal width. Typical primary time intervals have a width in the order of several tenth of microseconds. The total data collection time is usually several tenth of seconds.

In a further preferred embodiment, numbers of photon counts $\{\mathbf{n}_i\}$ subject to determination of a distribution function $\vec{P}(\mathbf{n})$ in step b) are derived from numbers of photon counts in primary

time intervals $\{N_j\}$ by addition of numbers of photon counts from primary time intervals according to a predetermined rule. One might e.g. be interested in choosing numbers of photon counts $\{n_i\}$ subject to determination of a distribution function $\vec{P}(n)$ which are calculated from the numbers of photon counts in primary time intervals $\{N_j\}$ according to the rule $n_i = \sum_{k=1}^{M} N_{Mi+k}$, where M is an integer number expressing how many times the time interval in which $\{n_i\}$ is determined is longer than the primary time interval.

In a further embodiment, numbers of photon counts $\{n_i\}$ are derived from predetermined primary time intervals according to a rule in which primary time intervals are separated by a time delay. In particular, the following rule can be applied: $n_i = \sum_{k=1}^{M} (N_{Mi+k} + N_{M(i+L)+k})$, where M and L are positive integer numbers, $\{n_i\}$ are numbers of photon counts subject to determination of a distribution function $\vec{P}(n)$, and $\{N_j\}$ are the numbers of photon counts in primary time intervals.

In some cases, it might be preferred to determine not only a single distribution function in step b), but rather a set of distribution functions $\vec{P}(n)$. These can be determined according to a set of different rules, said set of distribution functions being fitted jointly in step c). As an example a set of distribution functions with different values of M and/or L might be fitted jointly.

Typical physical quantities which might be determined in step c) according to the present invention are concentration, specific brightness and/or diffusion coefficient of molecules or other particles.

In a further preferred embodiment, the generating function is calculated using the expression $G(\xi) = \exp[\int dq c(q) \int d^3r (e^{(\xi-1)qTB(r)} - 1)]$, where $c(q)$ is the density of particles with specific brightness q, T is the length of the counting interval, and $B(r)$ is the spatial brightness profile as a function of coordinates.

Applying the definition (8) to formula (6) with $c \to cdV$ and $q \to qB(\mathbf{r})$, the contribution from a particular species and a selected volume element dV can be written as

$$G_i(\xi; dV) = \exp[c_i dV(e^{(\xi-1)q_i TB(\mathbf{r})} - 1)]. \tag{9}$$

Therefore, the generating function of the total photon count number distribution can be expressed in a closed form

$$G(\xi) = \exp[\sum_i c_i \int (e^{(\xi-1)q_i TB(\mathbf{r})} - 1) dV]. \tag{10}$$

Numeric integration according to Eq. (9) followed by a fast Fourier transform is the most effective means of calculating the theoretical distribution $P(n)$ corresponding to a given sample (i.e., given concentrations and specific brightness values of fluorescent species). If one selects $\xi = e^{i\varphi}$, then the distribution $P(n)$ and its generating function $G(\varphi)$ are interrelated by the Fourier transform. Therefore, it is particularly preferred to select the argument of the generating function in the form $\xi = e^{-i\varphi}$ and to use a fast Fourier transform algorithm in calculation of the theoretical distribution of the number of photon counts out of its generating function.

When calculating the theoretical distribution $P(\mathbf{n})$ in step c) according to the present invention, the spatial brightness profile might be modeled by a mathematical relationship between volume and spatial brightness. In particular, one might model the spatial brightness profile by the following expression: $\frac{dV}{dx} = a_1 x + a_2 x^2 + a_3 x^3$, where dV denotes a volume element, x denotes logarithm of the relative spatial brightness, and a_1, a_2 and a_3 are empirically estimated parameters.

Some fluorescent species may have a significantly wide distribution of specific brightness. For example vesicles, which are likely to have a significantly broad size distribution and a random number of receptors, may have trapped a random number of labeled ligand molecules. In order to fit count number distributions for samples containing such kind of species, it is useful to

modify Eq. (10) in the following manner. The assumption is made that the distribution of brightness of particles q within a species is mathematically expressed as follows:

$$\rho(q) \propto q^{a-1} e^{-bq}. \tag{11}$$

This expression has been selected for the sake of convenience: all moments of this distribution can be analytically calculated, using the following formula:

$$\int_0^\infty x^a e^{-bx} dx = \frac{\Gamma(a+1)}{b^{a+1}}. \tag{12}$$

It is straightforward to derive the modified generating function of a photon count number distribution. One can rewrite Eq. (9) as follows:

$$G(\xi) = \exp[\sum_i c_i \int dV \int_0^\infty dq \rho(q;a_i,b_i)(e^{(\xi-1)qTB(r)} - 1)], \tag{13}$$

where

$$\rho(q;a,b) = \frac{b^a}{\Gamma(a)} q^{a-1} e^{-bq}. \tag{14}$$

The integral over q can be performed analytically:

$$G(\xi) = \exp\left\{\sum_i c_i \int dV \left[\left(\frac{b_i}{b_i - (\xi-1)TB(x)}\right)^{a_i} - 1\right]\right\}, \tag{15}$$

The parameters a_i and b_i are related to the mean brightness $\bar{q}_i$ and the width of the brightness distribution σ_i^2 by

$$a_i = \frac{\bar{q}_i^2}{\sigma_i^2}, \qquad b_i = \frac{\bar{q}_i}{\sigma_i^2}. \tag{16}$$

In the range of obtained count numbers, the probability to obtain a particular count number usually varies by many orders of magnitude, see for example the distribution of Fig. 1. Consequently, the variance of the number of events with a given count number has a strong dependence on the count number. To determine weights for least squares fitting, one may assume that light intensities in all counting intervals are independent. Under this assumption, one has a problem of distributing M events over choices of different count numbers n, each particular outcome having a given probability of realization, $P(n)$. Covariance matrix elements of the distribution can be expressed as follows:

$$\langle \Delta P(n) \Delta P(m) \rangle = \frac{P(n)\delta(n,m) - P(n)P(m)}{M}, \qquad (17)$$

where M is the number of counting intervals per experiment.

For a further simplification, one may ignore the second term on the right side of Eq. (17), which can be interpreted as a consequence of normalization. In this case, the weights simply equal to the inverse values of the diagonal covariance matrix elements

$$W_n = \frac{M}{P(n)}. \qquad (18)$$

Dispersion matrix (17) corresponds to the multinomial distribution of statistical realizations of histograms. The Poissonian distribution, with the constraint that the total number of counting intervals M is fixed, will lead to the multinomial distribution. This is the rationale behind using Poissonian weights as given in Eq. (18).

Let n_k be the expectation value of the number of events of counting k photons and let $N = \sum_k n_k$ be their sum. Let m_k be a statistical realization with $M = \sum_k m_k$. Assume that realizations m_0, m_1, K obey Poissonian statistics

$$P(m_0, m_1, \mathrm{K}) = \frac{[n_0, n_1, \mathrm{K}]^{[m_0, m_1, \mathrm{K}]}}{[m_0, m_1, \mathrm{K}]!} e^{-N}, \qquad (19)$$

where we have introduced the notation $n_0^{m_0} n_1^{m_1} \mathrm{K} \equiv [n_0, n_1, \mathrm{K}]^{[m_0, m_1, \mathrm{K}]}$ and $m_0! m_1! \mathrm{K} \equiv [m_0, m_1, \mathrm{K}]$. The probability of having the total of M events is

$$P(M) = \frac{N^M}{N!} e^{-N}. \qquad (20)$$

The conditional probability of having m_0, m_1, K events if there is a total of M events is

$$P(m_0, m_1, \mathrm{K} \mid M) \equiv \frac{P(m_0, m_1, \mathrm{K})}{P(M)} = \frac{M! [n_0, n_1, \mathrm{K}]^{[m_0, m_1, \mathrm{K}]}}{N^M [m_0, m_1, \mathrm{K}]!},$$

or

$$P(m_0, m_1, \mathrm{K} \mid M) \equiv C_{m_0, m_1, \mathrm{K}}{}^M [p_0, p_1, \mathrm{K}]^{[m_0, m_1, \mathrm{K}]}. \qquad (21)$$

This is the multinomial distribution where we have introduced:

$$p_k \equiv \frac{n_k}{M}$$

and $C_{m_0, m_1, \mathrm{K}}{}^M$ are multinomial coefficients.

In general, a linear or linearized least squares fitting returns not only the values of the estimated parameters, but also their covariance matrix, provided the weights have been meaningfully set. It may turn out to be possible to express the statistical errors of the estimated parameters analytically in some simple cases (e.g., for the rectangular sample profile and single species) but in applications at least two-component analysis is usually of interest. Therefore, one may be satisfied with the numerical calculations of statistical errors. In addition to the „theoretical" errors with the assumption of non-correlated measurements (Eq. (17)), in some cases statistical errors have been estimated empirically, making a series of about a hundred FIDA experiments on identical conditions. As a rule, empirical errors are higher than theoretical ones by a factor of three to four. Empirical errors appear to be closer to the theoretical ones in scanning experiments. Therefore we are convinced that the main reason

of the underestimation of theoretical errors is the assumption of non-correlated measurements. Table 1 compares statistical errors of parameters estimated by fitting a photon count number distribution (FIDA) according to the present invention and by the moment analysis. Error values are determined through processing a series of simulated distributions. The present invention is overwhelmingly better than the moment analysis if the number of estimated parameters is higher than three.

Table 1

Data collection time, s	Primary time interval, µs	Number of species	Number of estimated parameters	Parameter specification	Value (qs in kHz)	Percent error of FIDA (inventi-on)	Percent error of moment analysis
10.0	40.0	1	2	c	0.5	0.59	0.54
				q	60.0	0.56	0.51
10.0	40.0	2	3	c_1	0.05	2.00	2.71
				q_1	150.0	1.54	1.89
				c_2	3.0	0.53	0.62
				q_2	5.0 (fixed)		
10.0	40.0	2	4	c_1	0.05	2.26	4.99
				q_1	150.0	1.63	2.53
				c_2	3.0	3.18	17.8
				q_2	5.0	3.35	14.9

Confocal techniques may be applied to a wide field of applications, such as biomedicine, diagnostics, high through-put drug screening, sorting processes such as sorting of particles like beads, vesicles, cells, bacteria, viruses etc.. The conjugate focal (confocal) technique is based on using a point source of light sharply focused to a diffraction-limited spot on the sample. The emitted light is viewed through a spatial filter (pinhole) that isolates the viewing

area to that exactly coincident with the illuminating spot. Thus, the illumination and detection apertures are optically conjugated with each other. Light originating from focal planes other than that of the objective lens is rejected, which effectively provides a very small depth of field. Therefore, in a particular preferred embodiment of the present invention, in step a) a confocal microscope is used for monitoring the intensity of fluorescence. In order to achieve a high signal-to-noise ratio, it is useful to monitor the intensity of fluorescence using an apparatus that comprises: a radiation source (12) for providing excitation radiation (14), an objective (22) for focussing the excitation radiation (14) into a measurement volume (26), a detector (42) for detecting emission radiation (30) that stems from the measurement volume (26), and an opaque means (44) positioned in the pathway (32) of the emission radiation (30) or excitation radiation (14) for erasing the central part of the emission radiation (30) or excitation radiation (14). It might be particularly preferred to use an optical set-up described in detail in **Figure 9**.

In a further preferred embodiment, the method according to the present invention is applied to fit a joint distribution of photon count numbers. In experiments, fluorescence from a microscopic volume with a fluctuating number of molecules is monitored using an optical set-up (e.g. a confocal microscope) with two detectors. The two detectors may have different polarizational or spectral response. In one embodiment, concentrations of fluorescent species together with two specific brightness values per each species are determined. The two-dimensional fluorescence intensity distribution analysis (2D-FIDA) if used with a polarization cube is a tool which can distinguish fluorescent species with different specific polarization ratios. This is a typical example of a joint analysis of two physical characteristics of single molecules or other particles, granting a significantly improved reliability compared to methods focussed on a single physical characteristic.

In order to express the expected two-dimensional distribution of the number of photon counts, it is favourable to use the following assumptions: (A) Coordinates of particles are random and independent of each other. (B) Contribution to fluorescence intensity from a particle can be expressed as a product of a specific brightness of the particle and a spatial brightness profile function characteristic to the optical equipment. (C) A short counting time interval T is

selected, during which brightness of fluorescent particles does not significantly change due to diffusion.

At first, a joint distribution of count numbers from a single fluorescent species and a single small open volume element dV is expressed. The volume element is characterized by coordinates $\mathbf{r}$ and spatial brightness $B(\mathbf{r})$, and the fluorescent species is characterized by its specific brightness values q_1 and q_2. By q_1 and q_2, mean photon count rates by two detectors from a particle situated at a point where $B(\mathbf{r}) = 1$ are denoted. A convenient choice is to select a unit of B, as usual in FCS, by the equation $\chi_1 = \chi_2$, where $\chi_k = \int B^k(\mathbf{r})d^3\mathbf{r}$. If the volume element happens to contain m particles, then the expected photon count numbers per time interval T from the volume element are $mq_1TB(\mathbf{r})$ and $mq_2TB(\mathbf{r})$, while the distribution of numbers of photon counts from m particles $P(n_1, n_2 \mid m)$ is Poissonian for both detectors independently:

$$P(n_1,n_2 \mid m) = \frac{(mq_1TB(x))^{n_1}}{n_1!} e^{-mq_1TB(x)} \frac{(mq_2TB(x))^{n_2}}{n_2!} e^{-mq_2TB(x)}. \qquad (22)$$

From the other side, under assumption (A), the distribution of the number of particles of given species in the volume element is Poissonian with mean cdV, c denoting concentration:

$$P_{dV}(m) = \frac{(cdV)^m}{m!} e^{-cdV}. \qquad (23)$$

The overall distribution of the number of photon counts from the volume element can be expressed using Eqs.22 and 23:

$$P_{dV}(n_1,n_2)=\sum_m P_{dV}(m)P(n_1,n_2\mid m)$$
$$=\sum_m \frac{(cdV)^m}{m!}e^{-cdV}\frac{(mq_1TB(\mathbf{r}))^{n_1}}{n_1!}e^{-mq_1TB(r)}\frac{(mq_2TB(\mathbf{r}))^{n_2}}{n_2!}e^{-mq_2TB(r)} \quad (24)$$

As in the one-dimensional case described above, a useful representation of a distribution of numbers of photon counts $P(n_1,n_2)$ is its generating function, defined as

$$G(\xi_1,\xi_2)=\sum_{n_1=0}^{\infty}\sum_{n_2=0}^{\infty}\xi_1^{n_1}\xi_2^{n_2}P(n_1,n_2). \quad (25)$$

The generating function of the distribution expressed by Eq 24 can be written as

$$G_{dV}(\xi_1,\xi_2)=e^{-cdV}\sum_m\frac{(cdV)^m}{m!}e^{-mq_1BT}e^{-mq_2BT}\sum_{n_1}\frac{(m\xi_1qBT)^{n_1}}{n_1!}\sum_{n_2}\frac{(m\xi_2qBT)^{n_2}}{n_2!}$$
$$=e^{-cdV}\sum_m\frac{\{cdV\exp[(\xi_1-1)q_1BT]\exp[(\xi_2-1)q_2BT]\}^m}{m!} \quad (26)$$
$$=\exp\left[cdV\left(e^{(\xi_1-1)q_1BT}e^{(\xi_2-1)q_2BT}-1\right)\right]$$

In particular, if one selects $\xi_k=\exp(i\varphi_k)$, then the distribution $P(n_1,n_2)$ and its generating function $G(\varphi_1,\varphi_2)$ are interrelated by a 2-dimensional Fourier transform. What makes the generating function attractive in photon count number distribution analysis is the additivity of its logarithm: logarithms of generating functions of photon count number distributions of independent sources, like different volume elements as well as different species, are simply added for the calculation of the combined distribution. Therefore, the generating function of the overall distribution of the number of photon counts can be expressed in a closed form:

$$G(\xi_1,\xi_2) = \exp[(\xi_1 - 1)\lambda_1 T + (\xi_2 - 1)\lambda_2 T + \sum_i c_i \int\left(e^{(\xi_1-1)q_{1i}TB(\mathbf{r})} e^{(\xi_2-1)q_{2i}TB(\mathbf{r})} - 1\right)d^3\mathbf{r}]. \quad (27)$$

In this formula, a contribution from background count rates, λ_1 by detector 1 and λ_2 by detector 2, as well as contributions from different fluorescent species, denoted by the subscript *i*, have been integrated. Numeric integration according to Eq. 27 followed by a fast Fourier transform is a very efficient means for calculation of the theoretical distribution $P(n_1,n_2)$ corresponding to a given sample (i.e. given concentrations and specific brightness values of fluorescent species).

The spatial brightness function is accounted through the spatial integration on the right side of Eq. 27. The three-dimensional integration can be reduced to a one-dimensional one by replacing three-dimensional coordinates r by a one-dimensional variable, a monotonic function of the spatial brightness $B(\mathbf{r})$. A convenient choice of the variable is $x = \ln[B(0) / B(\mathbf{r})]$. A sufficiently flexible model of the spatial brightness profile is presented by the following expression:

$$\frac{dV}{dx} \propto x(1 + a_1 x + a_2 x^2). \quad (28)$$

In the interval of obtained count numbers, the probability to obtain a particular pair of count numbers usually varies by many orders of magnitude. Consequently, the variance of the experimental distribution has also a strong dependence on the count numbers. To determine weights for least squares fitting, for simplification it is assumed that coordinates of particles in all counting intervals are randomly selected. (This means one ignores correlations of the

coordinates in consecutive counting intervals.) Under this assumption, one has a problem of distributing M events over choices of different pairs of count numbers n_1, n_2, each particular outcome having a given probability of realization, $P(n_1,n_2)$. Covariance matrix elements of the distribution can be expressed as follows:

$$\langle \Delta P(n_1,n_2)\Delta P(n'_1,n'_2)\rangle = \frac{P(n_1,n_2)\delta(n_1,n'_1)\delta(n_2,n'_2) - P(n_1,n_2)P(n'_1,n'_2)}{M}, \qquad (29)$$

where M is the number of counting intervals per experiment.

For a further simplification, one may ignore the second term on the right side of Eq. (29), which can be interpreted as a consequence of normalization. In this case, the weights simply equal to the inverse values of the diagonal covariance matrix elements

$$W(n_1,n_2) = \frac{M}{P(n_1,n_2)}. \qquad (30)$$

In general, a linearized least squares fitting algorithm returns not only values of estimated parameters, but also their covariance matrix, provided weights have been meaningfully set. In addition to "theoretical" errors corresponding to the assumption of uncorrelated measurements (Eq. (30)), in some cases statistical errors have been determined empirically, making a series of about 100 2D-FIDA experiments at identical conditions. As a rule, empirical errors are higher than theoretical ones by a factor of three to four. The main reason of underestimation of theoretical errors is most likely the assumption of uncorrelated measurements.

Even though the assumption of uncorrelated measurements yields underestimated error values, it is a very useful theoretical approximation, allowing to compare accuracy of analysis under different experimental conditions as well as different methods of analysis. Also, this approximation provides an easy method of data simulation which is a useful tool in general. A simple and very fast method of data simulation is calculation of the expected event number as a function of photon count numbers and addition of random Poisson noise to each event number independently.

In Table 2 theoretical errors of one-dimensional and two-dimensional fluorescence intensity distribution analysis according to the present invention are presented in two selected cases of two fluorescent species. In both cases the ratio of specific brightness values of the two species is three. In the case of 2D-FIDA, it is assumed that spectral sensitivities of the two detectors are tuned to different species. In both cases data collection time of 10 s, time window of 40 μs and background count rate of 1 kHz are assumed. Note that the statistical errors of the estimated parameters are significantly lower in the 2D-FIDA example.

Table 2

Method	Parameter specification	Parameter value (selected)	Percent error
1D-FIDA (according to the invention)	c_1V	0.5	6.6
	c_2V	0.5	4.9
	q_1	60 kHz	2.2
	q_2	20 kHz	10.2
2D-FIDA (according to the invention)	c_1V	0.5	1.1
	c_2V	0.5	1.1
	q_{A1}	60 kHz	0.77
	q_{A2}	20 kHz	1.2
	q_{B1}	20 kHz	1.2
	q_{B2}	60 kHz	0.77

The two-dimensional fluorescent intensity distribution analysis according to the present invention is in the following compared to the prior art moment analysis.

Factorial moments of the distribution $P(n_1,n_2)$ are defined as

$$F_{kl} = \sum_{n_1,n_2} \frac{n_1!n_2!}{(n_1-k)!(n_2-l)!} P(n_1,n_2). \tag{31}$$

Factorial moments are related to factorial cumulants K_{kl}

$$K_{kl} = F_{kl} - \sum_{\substack{i,j \\ i+j>0}} C_i^{k-1} C_j^l K_{k-i,l-j} F_{ij}. \tag{32}$$

C denotes binomial coefficients. Cumulants can be expressed through concentrations and specific brightness values by a simple relation

$$K_{kl} = \chi_{k+l} T^{k+l} \sum_i c_i q_{1i}^k q_{2i}^l. \tag{33}$$

If the unit of B is selected by the equation $\chi_1 = \chi_2$, χ_1 has the meaning of the sample volume, denoted by V, and Eq. 33 can be written as

$$\gamma_{k+l} K_{kl} = \sum_i (c_i V)(q_{1i} T)^k (q_{2i} T)^l. \tag{34}$$

where γ denotes a series of constants characterizing the brightness profile:

$$\gamma_m = \frac{\chi_1}{\chi_m}. \tag{35}$$

The principle of moment analysis is to determine values of a few cumulants from an experiment and solve a system of Eqs. 33 in respect to unknown concentrations and brightness values.

In Table 3 statistical errors of 2D-FIDA (present invention) and 2D-MAFID (prior art) are presented determined by generating a series of 30 random distributions of count numbers, simulated for identical "samples", thereafter applying 2D-FIDA and 2D-MAFID, and determining the variance of estimated parameters in both cases. Note a tendency that the

advantages of 2D-FIDA compared to 2D-MAFID increase with the number of parameters to be estimated.

Table 3

Data collection time, s	Number of species	Number of estimated parameters	Specification of cumulants used in MAFID	Specification of parameters	True values	Percent error of FIDA	Percent error of MAFID
2	1	3	K_{01}	cV	0.5	1.1	1.3
			K_{10}	q_A	60 kHz	1.2	1.5
			K_{11}	q_B	40 kHz	1.3	1.6
10	2	4	K_{01}	c_1V	0.5	1.1	2.5
			K_{10}	c_2V	0.5	1.0	4.2
			K_{02}	q_{A1}	60 kHz	0.70	1.2
			K_{20}	q_{A2}	20 kHz	(fixed)	(fixed)
				q_{B1}	40 kHz	1.3	5.7
				q_{B2}	80 kHz	(fixed)	(fixed)
10	3	5	K_{01}	c_1V	0.2	2.0	2.4
			K_{10}	c_2V	0.2	1.2	1.2
			K_{02}	c_3V	0.2	1.6	1.9
			K_{11}	q_{A1}	40 kHz	1.4	1.8
			K_{20}	q_{A2}	20 kHz	(fixed)	(fixed)
				q_{A3}	60 kHz	(fixed)	(fixed)
				q_{B1}	10 kHz	3.6	9.0
				q_{B2}	60 kHz	(fixed)	(fixed)
				q_{B3}	70 kHz	(fixed)	(fixed)
10	2	6	K_{01}	c_1V	0.5	1.1	4.3
			K_{10}	c_2V	0.5	1.0	5.0
			K_{02}	q_{A1}	60 kHz	0.70	1.4
			K_{11}	q_{A2}	20 kHz	1.3	4.5
			K_{20}	q_{B1}	40 kHz	0.90	2.9
			K_{21}	q_{B2}	80 kHz	0.55	1.5

Error values are calculated from the scattered results of analysis applied to a series of simulated data.

In Table 4 the relative deviation of mean values (i.e, bias) of estimated parameters are presented for 2D-FIDA (present invention) and 2D-MAFID (prior art). In each case bias is determined from analysis of a series of thirty simulated random distributions of count numbers. Three cases were analysed. In the first case, models used in data simulations and data analysis were identical. In the second case, the distributions of count numbers were simulated assuming that particles of the second species are not equivalent but being distributed by their individual brightness with a relative half-width of 20 percent. This phenomenon was intentionally ignored in analysis, however. Of course, applying a slightly inadequate model for analysis produces bias of estimated parameters. The third case is similar to the second one except the relative half-width of the individual brightness distribution of the second species is 50 percent, which is a usual value for vesicular preparations. It is worth noting that methodological deviations are noticeable when mapping weighted residuals of 2D-FIDA in cases two and three, but 2D-FIDA still returns meaningful results. 2D-MAFID is a more sensitive method to model roughness.

Table 4

Parameter specification	True value (selected)	Bias of 2D-FIDA, percent			Bias of 2D-MAFID, percent		
		Case 1	Case 2	Case 3	Case 1	Case 2	Case 3
c_1V	1.0	+0.1 ±0.2	-0.35	-2.0	+0.1 ±0.2	-6.5	-28
c_2V	0.05	+0.6 ±0.4	-2.0	-10.6	+1.8 ±0.6	-15.6	-69
q_{A1}	20 kHz	-0.1 ±0.2	+0.8	+5.0	-0.3 ±0.3	+10.0	+58
q_{A2}	100 kHz	-0.3 ±0.4	-0.7	-11.2	-0.9 ±0.3	+5.5	+41
q_{B1}	1 kHz	-1.2 ±0.5	+2.6	+20.6	-6.7 ±3.0	+75	+563
q_{B2}	200 kHz	-0.3 ±0.4	+1.2	+1.3	-0.9 ±0.3	+11.6	+99

BRIEF DESCRIPTION OF FIGURES

Figure 1 shows a count number distribution obtained for a solution of the dye tetramethylrhodamine **(a)** and residual curves corresponding to different fitting procedures **(b)**.

Figure 2 shows simulated distributions of the number of counts for a case which models a binding reaction of a labeled ligand to vesicles.

Figure 3 illustrates theoretical errors of the estimated parameters c and q of a solution of single species, depending on the value of q.

Figure 4 illustrates theoretical errors of the estimated parameters c and q of a solution of single species, depending on the value of c.

Figure 5 illustrates theoretical errors of the estimated parameters of c and q of a solution of single species, depending on the value of T.

Figure 6 illustrates theoretical errors of the estimated parameters c and q of a mixture of two species, depending on the value of T.

Figure 7 illustrates theoretical errors of the estimated parameters c and q of a mixture of two species, depending on the ratio of q_2 to q_1.

Figure 8 illustrates theoretical errors of the estimated parameters c and q of a mixture of two species, depending on concentrations.

Figure 9 illustrates an apparatus adapted for use in performing the method according to the present invention.

In **Figure 10A**, the calculated photon count number distributions, $P(n)$, for cases having identical mean count number $\bar{n}$ but differing by the composition of the sample are plotted.

Figure 10 B illustrates the distributions of the number of photon counts of pure solutions of rhodamine 6G (Rh6G) and tetramethylrhodamine (TMR), as well as a mixture of these two dyes.

The exemplary residuals for Rh6G are shown in **Figure 10 C**.

Figure 10 D shows the results of an ITR analysis (inverse transformation with the help of linear regularization and constraining concentrations to non-negative values) applied to the curves of Figure 10 B.

Figure 11 shows an ITR analysis of hybridized **(A-C)** and restriction enzyme cleaved **(D, E)** labeled oligonucleotides. The curves result from a set of 20 individual 10 s measurements which show variations among each other of less than 10 %.

Figure 12 illustrates hybridization and restriction enzyme cleavage of different combinations of labeled and unlabeled oligonucleotides.

Figure 13 is a graphical presentation of a joint distribution of the number of photon counts measured for a solution of TAMRA.

Figure 14 is a graphical presentation of weighted residuals of a joint distribution of count numbers obtained from a mixture of TAMRA (5'-(6'-carboxytetramethylrhodamine) and RRX (rhodamine red X).

Figure 15 illustrates joint distributions of the numbers of photon counts for the "parallel" and "perpendicular" polarization components of fluorescence measured for equal theophylline concentration of 2 nM, but different antibody concentrations.

Figure 16 illustrates the results of 2D-FIDA applied to data from samples of equal theophylline concentration, but different antibody concentration.

Figure 17 illustrates the principle of a two-color 2D-FIDA experiment with multiple binding sites per vesicle.

Figure 18 illustrates joint distributions of the numbers of photon counts in "green" and "red" measured in conditions of high (A) and low (B) degree of binding of SMS-14 (somatostatin-14) to SSTR-2 (human type-2 high-affinity somatostatin receptor).

Figure 19 shows the competition curve of the binding reaction of SMS-14 to SSTR-2.

Figure 20 illustrates an embodiment in which numbers of photon counts $\{\mathbf{n}_i\}$ subject to determination of a distribution function $\bar{P}(\mathbf{n})$ in step b) are derived from numbers of photon counts in primary time intervals $\{\mathbf{N}_j\}$ by addition of numbers of photon counts from primary time intervals according to a predetermined rule.

Figure 21 illustrates a further embodiment in which numbers of photon counts $\{\mathbf{n}_i\}$ are derived from predetermined primary time intervals according to a rule in which primary time intervals are separated by a time delay.

Figure 22 shows a schematic diagram of binding of a fluorescently-labelled molecule to receptor-bearing vesicles as observed utilizing the present invention.

Figure 23 illustrates the ligand binding characteristics of TMR-EGF to membranes prepared from A431 cells.

Figure 24 shows the binding of TMR-EGF to membranes prepared from HCT cells..

Figure 25 illustrates the pharmacological profile of the EGF receptor.

Figure 26 illustrates the ligand binding characteristics of Bodipy FL-CGP 12177.

Figure 27 shows the inhibition of Bodipy FL-CGP 12177 binding in 40 µl and 1 µl assay volumes.

DETAILED DESCRIPTION OF FIGURES

Reference is now made to **Figure 1** which shows a count number distribution obtained for a solution of the dye tetramethylrhodamine **(a)** and three residuals curves corresponding to the best fit obtained with Eqs (36), (37), and (38) below **(b)**. The concentration of the aqueous tetramethylrhodamine solution was about 10^{-9} M. Primary time intervals were 40 µs. The data collection time was 60 s.

The most widely used spatial profile model in FCS is the three-dimensional Gaussian profile with a single parameter of shape, the axial dimension ratio in longitudinal and radial directions. Residuals curve with open circles illustrates the fit quality obtainable with the Gaussian profile. There are large systematic deviations in residuals. What is a sufficiently flexible model for fitting FCS data has turned out to be a rather inflexible and inadequate model for FIDA.

A model of the sample profile which has yielded a better fit of the measured distribution $\bar{P}(n)$ is Gaussian-Lorentzian (open squares), but this model still lacks flexibility. According

to Eq. (8), a certain function of the spatial brightness B is integrated over the volume. In other words, it is a relationship between B and V, characterizing a given spatial brightness profile in FIDA. For example, the Gaussian profile yields the relationship

$$\frac{dV}{dx} \propto \sqrt{x}, \tag{36}$$

where $x = -\ln B$. The Gauss-Lorentzian profile yields the relationship

$$\frac{dV}{dx} \propto e^{x/4}\sqrt{\sinh\frac{x}{2}}. \tag{37}$$

Both of the relationships are rather inflexible, i.e., they do not provide any spatial shape parameters to adjust the theoretically calculated distribution to fit the measured data.

When looking for sufficiently flexible models to fit experimental data, it might be useful to apply the following relationship:

$$\frac{dV}{dx} \propto (x + a_1x^2 + a_2x^3). \tag{38}$$

There is a formal rather than a physical model behind Eq. (38). The fit quality obtainable with Eq. (38) is illustrated by the filled squares curve.

Referring now to **Figure 2**, simulated distributions of the number of counts are shown for a case which models a binding reaction of a labeled ligand to vesicles. Primary time intervals were 40 µs, values of the spatial parameters of Eq. (38) a_1 = -0.4; a_2 = 0.08, background count rate b = 1.0 kHz, data collection time 4 s. Curve „ligand" corresponds to a species of c = 6.0; q = 6.0 kHz/particle; σ_q = 0. Curve „vesicles" corresponds to a species of c = 0.05; q = 300.0 kHz/particle; σ_q = 150.0. Curve „mixture" corresponds to their mixture. Concentrations and specific brightness values have been selected to model a characteristic situation in drug screening. Fitting of curve (c) returns the values of the five parameters characterizing the given „sample" with statistical errors which are mostly between 3.5 and 6 percent, except the

error of σ_q of vesicles which is 13 percent. If, however, σ_q of vesicles is fixed in fitting, all the statistical errors are below 4 percent.

For the fastest data simulation algorithm, one may calculate the expected distribution and generate a random Poisson number of events for each value of n independently. Generation of a random Poisson number is the following: For a given expected value of events E, a simulated number of events S is determined from a routinely generated number R between 0.0 and 1.0 through inequations

$$\sum_{i=0}^{S-1} \text{Poisson}(i; E) < R \leq \sum_{i=0}^{S} \text{Poisson}(i; E)$$

As a cosmetic error, the total number of events $\sum_n S(n)$ may slightly deviate from the pre-given number M. A slower but a straightforward data simulation algorithm is the generation of a random configuration of particles in volume elements contributing to fluorescence, the calculation of the classical light intensity corresponding to the given configuration of particles, and the generation of a random Poisson number corresponding to this intensity, as a simulated number of photon counts. This procedure is repeated M times to obtain a simulated count number distribution.

Reference is now made to **Figure 3** which illustrates the theoretical errors of the estimated parameters c and q of a solution of single species, depending on the value of q. The following values of experimental parameters were selected: $c = 1.0$; $T = 20$ µs; $a_1 = -0.4$; $a_2 = 0.08$; $b = 1.0$ kHz; data collection time 2 s.

Figure 4 illustrates the theoretical errors of the estimated parameters c and q of a solution of single species, depending on the value of c. The following values of experimental parameters were selected: $q = 60$ kHz/particle; $T = 20$ µs; $a_1 = -0.4$; $a_2 = 0.08$; $b = 1.0$ kHz; data collection time 2 s.

Referring now to **Figure 5**, theoretical errors of the estimated parameters c and q of a solution of single species are shown, depending on the value of T. The following values of experimental parameters were selected: $c = 1.0$; $q = 30.0$ kHz/particle (upper graphs); $q = 60.0$ kHz/particle (lower graphs); $a_1 = -0.4$; $a_2 = 0.08$; $b = 1.0$ kHz; data collection time 2 s.

Figure 6 illustrates the theoretical errors of the estimated parameters c and q of a mixture of two species, depending on the value of T. The following values of experimental parameters were selected: $c_1 = 0.1$; $c_2 = 2.0$; $q_1 = 200.0$ kHz/particle; $q_2 = 10.0$ kHz/particle; $a_1 = -0.4$; $a_2 = 0.08$; $b = 1.0$ kHz; data collection time 10 s. Note that the optimal value of T for the determination of the parameters of the brighter species is lower than that of the darker species.

Reference is now made to **Figure 7** which illustrates the theoretical errors of the estimated parameters c and q of a mixture of two species, depending on the ratio of q_2 to q_1. The following values of experimental parameters were selected: $q_1 = 50.0$ kHz/particle; $c_1 = c_2 = 0.5$; $a_1 = -0.4$; $a_2 = 0.08$; $b = 1.0$ kHz; data collection time 40 s.

Figure 8 illustrates the theoretical errors of the estimated parameters c and q of a mixture of two species, depending on concentrations. The concentrations were changed synchronously, $c_1 = c_2$. The following values of experimental parameters were selected: $q_1 = 75.0$ kHz/particle; $q_2 = 25.0$ kHz/particle; $a_1 = -0.4$; $a_2 = 0.08$; $b = 1.0$ kHz; data collection time 60 s. Note that an optimal concentration exists at about one particle per sample volume. This is generally true, except if less than three parameters are to be determined.

Reference is now made to **Figure 9** which shows one embodiment of an apparatus adapted for use in performing the method according to the present invention. Apparatus **10** comprises a laser **12** which serves as a light source for illuminating the sample by a bundle of coherent, monochromatic excitation radiation **14**. Excitation radiation **14** is paralleled by a lens **16** and reaches a dichroic mirror **20**. Preferably, the angle between the optical axes **18** and the dichroic mirror **20** is 45°. The dichroic mirror **20** reflects the excitation radiation **14** in direction of an objective lens **22** having its focus **24** within a sample volume **26**. Sample volume **26** and objective lens **22** are preferably separated from each other by a transparent cover glass **28**, e. g. by the bottom of a commercially available micro-titer plate which houses the sample. The sample preferably includes fluorescently labelled molecules or other particles. Due to excitation by an appropriate excitation radiation **14**, the molecules or other particles present in the sample emit radiation **30**. Emission radiation **30** passes the objective lens **22** and reaches the dichroic mirror **20** which is transparent for emission radiation **30**. Thereafter, emission radiation passes a filter **34** and a collimator lens **36** on the optical axes **32**. A pinhole **38** is situated in the focus of collimator lens **36**. Emission radiation **30** passing the pinhole **38**

reaches a further lens **40** and, thereafter, is detected by the photo-detector **42**. Within the pathway of emission radiation **30**, in particular between dichroic mirror **20** and photo-detector **42**, an opaque means **44** is provided through which a central part of the emission radiation **30** cannot pass. This central part of the emission radiation **30** stems from areas on the optical axes **32** in front of or behind the focus **24** of the excitation radiation **14**. Only emission radiation **30** that stems from the focus **24** or its direct neighbourhood passes the pinhole **38** and reaches photo-detector **42**. Instead of placing an opaque means **44** within the pathway of emission radiation **30**, the pathway of excitation radiation **14** is also suitable for positioning an opaque means **44**. In particular, an opaque means **44** can be positioned between laser **12** and dichroic mirror **20**. Use of an opaque means **44** as described in detail herein improves the signal-to-noise ratio.

In **Figure 10A**, the calculated photon count number distributions, $P(n)$, for five cases of equal mean count rate, $\bar{n} = 1.0$ are shown. The open symbols correspond to solutions of single species, but with different values of the mean count number per particle qT. The solid line is calculated for a mixture of two species, one with $qT = 0.5$ and the other with $qT = 8.0$. Obviously, the curves differ from each other considerably. The important point is that FIDA according to the present invention can unambiguously separate the contributions of the individual species.

Reference is now made to **Figure 10 B** which illustrates the distributions of the number of photon counts of pure solutions of two different dyes, 0.5 nM rhodamine 6G (Rh6G) and 1.5 nM tetramethylrhodamine (TMR), as well as a mixture of the two (0.8 nM TMR, 0.1 nM Rh6G). The main equipment is a confocal microscope (ConfoCor®; EVOTEC BioSystems and Carl Zeiss, Germany) routinely used for fluorescence correlation studies. An attenuated (to about 800 μW) beam from an argon ion laser, wavelength 514.5 nm, is focussed to a spot of approximately 0.5 μm radius, which is twice the size of a spot in usual FCS experiments, and results in a diffusion time of approximately 200 μs for rhodamine 6G. The excitation intensity has generally been kept lower than or equal to a level characterized by about 15 percent amplitude of the triplet term of the auto-correlation function. Fluorescence emission is detected through a pinhole on the focal plane of the microscope using an avalanche photodiode detector SPCM-AQ 131 (EG&G). The distributions of the number of photon counts were measured at T = 40 μs dwell time. Data collection time was 50 s. These

distributions serve as input data for FIDA. The results of a multi-component fit analysis are given in Table 5 below with χ^2 values calculated according:

$$\chi^2 = \frac{\sum W_n [\hat{P}(n) - P(n)]^2}{n_P - n_{fit}}, \tag{39}$$

where n_p is the length of the measured distribution $\hat{P}(n)$, and n_{fit} is the number of fit parameters. In said multi-component analysis one fits the measured distribution function of number of photon counts, assuming a certain number of fluorescent species, and estimates unknown concentration and specific brightness values.

Table 5

Sample	a_2	a_3	C	q (kHz)	χ^2
Rh6G	-0.380 ±0.009	0.077 ±0.003	0.461 ±0.003	107.2 ±0.8	0.97
TMR	-0.427 ±0.032	0.084 ±0.014	1.517 ±0.012	36.56 ±0.29	0.81
Mixture	-0.380 (fixed)	0.077 (fixed)	0.103 ±0.012 0.738 ±0.011	109.1±4.0 37.4 ±1.0	0.77

In all cases, the background count rate was fixed to the value of 1.05 kHz, as measured with de-ionized water. a_2 and a_3 are pre-normalization values when a_1 is fixed to 1.0. The theoretical statistical errors in Table 5 correspond to theoretical weights:

$$W_n = \frac{N}{P(n) + \frac{1}{N}}. \qquad (40)$$

This formula is derived under a simple assumption of N independent measurements of the number of photon counts. In reality, consecutive measurements are correlated, therefore the errors of estimated parameters returned by the fitting algorithm underestimate real statistical errors. We have empirically determined from a separate series of 30 to 200 measurements that these statistical errors are greater than theoretical ones by a factor of about three.

The exemplary residuals for Rh6G are shown in **Figure 10 C**.

The results of ITR analysis are shown in **Figure 10 D** expressing the distribution of the number of particles as a function of their specific brightness. Such ITR analysis is an inverse transformation realized with the help of linear regularization and constraining concentrations to non-negative values. ITR is a valuable tool especially for samples from which either no *a priori* information about the sample composition is given or where the sample composition is heterogeneous. The dashed lines correspond to the solutions of the single dyes (Rh6G and TMR) and the solid line to their mixture. The ordinates give the mean number of particles within the confocal volume element (left: single dyes; right: mixture). For equipment details see description of Figure 10B. The ideal outcome would be single δ-peaks for the solutions of

single species and two δ-peaks for the mixture. In reality, the width of the ITR output spectral peaks is determined not only by the true width of the distribution of specific brightness values but also by the accuracy of input data and the particular realization of the linear regularization: simply, if a broad spectrum fits experimental data as well as a narrow one then ITR prefers the broad one.

As a further example, the method according to the present invention has been applied to study the hybridization of 5'-(6-carboxytetramethylrhodamine (TAMRA))-labeled 40mers with either labeled or non-labeled complementary oligonucleotides and the subsequent symmetrical cleavage of the DNA hybrid by the restriction endonucleases *Hind III* and *Kpn I*. The specific oligonucleotides used in this study were

TAMRA-AAGAAGGGGTACCTTTGGATAAAAGAGAAGCTTTTCCCGT(5'-TAMRA-Oligo A) and

TAMRA-ACGGGAAAAGCTTCTCTTTTATCCAAAGGTACCCCTTCTT(5'-TAMRA-Oligo B).

They were purchased in HPLC pure quality from Applied Biosystems (Weiterstadt, Germany). All measurements were carried out on the above described FCS reader at excitation/emission wavelengths of 543/580 nm using a 4 mW helium/neon laser (Uniphase) attenuated to approximately 300 µW. The water background was found to be below 800 Hz. For the measurements, sample aliquots were diluted to 1 nM and 20 µl were assayed in a 8-well chambered coverglass (Nalge Nunc) at room temperature. The hybridization reaction was performed in 70% formamide containing 10mM Tris/HCl buffer (pH 8.0), 1mM EDTA, 0.2mM NaCl and an oligonucleotide concentration of 0.5µM. Denaturation was at 95°C for 2 min and subsequent hybridization was at 55-60°C for 40 min in accordance with the optimized temperature Tx which is 10-15 degrees below the melting point Tm (Heating block, Techne). Tm was calculated as follows: Tm = 81.5 +16.6 (log10[Na+]) + 0.41 (%G+C) - 600/N (N = 40; %G+C = 42.5). Restriction digest analyses of the hybrid DNA were performed by the restriction enzymes *Hind* III and *Kpn* I. The restriction site was chosen in order to obtain fragments of different size. The cleavage reactions were performed in 3.3mM tris/acetate (pH 7.9), 1 mM magnesium acetate, 6.6. mM potassium acetate and 0.1mg/ml bovine serum albumin at 37°C for 1h. The reaction course is characterized by significant shifts of the fluorescence intensity per molecule within a range of one order of magnitude (**Figures 11 A - E**). It is important to note that the resulting double product peak corresponds

to one single hybridization species in which no none-hybridized species are detectable. This could be easily demonstrated in hybridization/cleavage experiments using labeled/nonlabeled oligonucleotide combinations where signals with different brightness compared with the double labeled hybrid have been obtained (Fig. 12 A,B). One explanation for such a double-peak structure could be conformational fluctuations resulting from transitions between two conformational states. This behavior is described using a three-state model of the conformational dynamics with a polar, a nonpolar, and a quenching environment of the label (Eggeling et al., Proc. Natl. Acad. Sci. USA 95: 1556 - 1561). From the present data it can be concluded that the conformational fluctuations are significantly dependent on the DNA length and the number of labels. The small digested DNA fragments exhibit a single brightness and the concentration ratio of the educt double peaks shifts toward one component when one-label hybrids are studied. As a further result, small fragments show low molecular brightness and large fragments correspond to high brightness values ($Q_2 \approx Q_3$, $Q_1 \approx Q_4$).

Based on symmetrical cleavage sites for both enzymes DNA fragments of equal size and subsequently very similar molecular brightness are to be expected. **Figures 12 A and B** clearly illustrate that such a result has been observed and the theoretical relationship $Q_1 + Q_2 = Q_3 + Q_4$ is experimentally confirmed. Restriction digest analyses of the hybrid DNA were performed with the restriction enzymes Hind III and Kpn I either alone or in combination. The restriction sites lead to symmetrically cleaved fragments (2x12 mers, 1x16 mer for double digest). [•] corresponds to labeled DNA. Q_{01-03}: intensities of DNA hybrids, Q_i: intensities of cleavage products. The bulk of all the measurements of cleavage products using single and doubly labeled DNA structures makes it possible to classify all observed intensities with individual structures in a single measurement – a property of the method of the present invention which is not possible using any other known analytical method.

Reference is now made to **Figures 13** and **14**. As the central optical part of the equipment for 2D-FIDA, a confocal microscope is used, like in FCS spectrometers (Koppel et al., Biophys. J. 16: 1315 – 1329, 1976). For excitation of fluorescence, a beam from an Ar or green He-Ne laser is attenuated by neutral filters, passes a beam expander and is directed to the microscope objective by a dichroic mirror. In a number of experiments with slowly diffusing particles, beam scanning in combination with sample scanning is used, as a tool known from laser

scanning microscopy. Fluorescence is collected by the same objective through the dichroic mirror, and is focussed to a confocal pinhole which serves to reject the out-of-focus light. Resolution in the longitudinal direction is additionally improved by using a concentrical opaque spot closing about a quarter of the aperture in the fluorescence collection path of the microscope (see description of **Figure 9**). The light which passes the pinhole is divided by a beamsplitter for detection by two detectors. Depending on the general type of a 2D-FIDA experiment, the beamsplitter is either a polarization cube, or a dichroic mirror. In the first case, a common spectral band-pass filter is used, while in the case of two-colour FIDA, each detector has a different band-pass filter in front of it. The photon counting detectors are silicon avalanche photodiode modules SPCM-AQ-131, EG&G Optoelectronics, Canada. The TTL pulses from the detectors are counted by a two-channel counter, constructed by EVOTEC BioSystems AG (Hamburg, Germany) as a plug-in card of a computer. The count number distributions are calculated during reading data from the 32 MB onboard buffer, which itself is an online process. By feeding the detector outputs to a correlator, FCS measurements can be performed in parallel with FIDA experiments.

The levels of background count rate for both detectors are determined by a separate experiment on bi-distilled water. The main contributor to the non-fluctuating background light intensity is Raman scattering from water.

The radius of the monitored sample volume can be adjusted by selecting an appropriate expansion factor of the original laser beam. The focal beam radius of about 0.6 µm is used yielding diffusion times for simple organic dye molecules (e.g., TAMRA) of about 260 µs, which is considered long compared to the 40 µs dwell time of counters, so that the approximation of constant molecular brightness during the counting interval is valid. The

excitation intensity is adjusted as a compromise between a high count rate per molecule and low population of the triplet state. The triplet state population was kept at about 15 percent level. Higher triplet population values might significantly distort the apparent spatial brightness profile. The population of the triplet state was measured with the correlator (ALV-5000, ALV, Langen, Germany) during the set-up of a series of experiments.

For methodological test experiments, two different dyes were selected, carboxytetramethyl-rhodamine (TAMRA) and rhodamine red X (RRX). These dyes have different emission spectra, as well as different extinction coefficients at the laser wavelength of 543.5 nm. In these experiments, a wideband 40/60 beamsplitter was used in front of the detectors. The spectral filter of the „red" channel has the center wavelength of 605 nm and FWHM of 50 nm while the corresponding figures for the „yellow-green" channel are 575 nm and 30 nm. The dyes were diluted in distilled water so that the average number of molecules in the observation volume was in the range of 0.5 to 2.0, corresponding to concentrations between 0.23 and 0.92 nM.

For each experiment, about 20 µl of the sample solution was placed on a coverslip separating the sample from the water immersion objective (Zeiss C-Apochromat 40x1.2 W Korr). Each distribution was collected for 60 seconds. Each of the dyes was measured separately, but also mixtures of the dyes with different concentration ratios were measured. The parameters describing the spatial brightness profile were determined from an experiment on TAMRA and were fixed in subsequent analysis of other samples at values $a_1 = -0.405$ and $a_2 = 0.0772$. Mixtures were measured and analyzed in order to see how well the method returns values of specific parameters of the two species.

As an example, **Figure 13** visualizes a count number distribution measured for a pure TAMRA solution. Values corresponding to the z-axis are logarithm values of the probability to obtain a given pair of count numbers n_1 and n_2. Fitting of the distribution returns mean number of particles, cV = 1.139 ±0.005, specific brightness for the „red" channel q_1 = 79.4 ±0.5 kHz, and for the „yellow-green" channel q_2 = 50.9 ±0.3 kHz. In Table 6, results of analysis of test experiments are presented. Samples have not been specified by concentration values calculated from dilution factors of the preparation because adsorption of dye molecules to glass surfaces influences real concentrations significantly. Because of the same reason, concentration values are not well reproduced from sample to sample; a shift of concentration values from realization to realization is also sometimes observable. Specific brightness values are well reproduced, however. Values of statistical errors presented are theoretical values corresponding to the assumption of uncorrelated measurements, multiplied by three, which is an empirical factor. In addition to statistical errors, deviations from sample to sample of a modest size are also noticeable.

Table 6

Sample	Realization number	Mean number of molecules per sample volume, cV	Specific brightness in „red", q_1, kHz	Specific brightness in „yellow-green", q_2, kHz
TAMRA	1	1.128 ±0.005	79.6 ±0.4	51.3 ±0.3
	2	1.139	79.4	50.9
	3	1.160	79.4	50.8
	4	1.171	79.0	50.6
RRX	1	1.892 ±0.009	48.0 ±0.3	15.63 ±0.09
	2	1.859	48.0	15.63
	3	1.850	47.3	15.44
	4	1.811	47.9	15.58

TAMRA and RRX	1	0.99 ±0.05	78.0 ±1.0	51.8 ±1.1
		1.14 ±0.05	49.1 ±1.1	15.0 ±0.9
	2	1.01	76.8	51.1
		1.08	49.5	15.1
	3	0.99	77.9	51.8
		1.03	49.3	15.1
	4	0.97	76.9	51.7
		1.03	50.0	15.5
TAMRA and RRX, new sample	1	0.93 ±0.07	74.6 ±1.3	49.6 ±1.5
		2.51 ±0.07	47.6 ±0.8	14.7 ±0.5
	2	0.98	75.2	49.2
		2.38	46.8	14.2
	3	0.96	75.0	49.4
		2.25	48.0	14.7
	4	0.94	76.1	49.9
		2.16	47.6	14.8

It is worth noting that distributions measured with mixtures are qualitatively different from those measured for pure dyes. **Figure 14** visualizes weighted residuals of fitting a distribution measured with a mixture of TAMRA and RRX. The upper graph corresponds to the adequate analysis when two species were assumed to be present; residuals are scattered quite randomly and uniformly. The lower graph corresponds to the assumption that only a single species is present; there is a significant difference between the measured and the calculated distribution in this case. n_1 is the count number obtained by the „red" detector, and n_2 is the count number obtained by the „yellow-green" detector.

In traditional fluorescence polarization studies, average intensities of two polarization components of fluorescence are directly measured. Fluctuations of the intensities are not of

direct interest there but are considered rather as a source of statistical errors. Changes in the fluorescence polarization values of a sample containing a fluorescently labeled binding partner reflect changes in molecular volume and, hence, provide direct information on equilibrium binding. Fluorescence polarization measurements can also be performed in real-time, allowing the kinetic analysis of association and dissociation reactions. One of the most widely-used fluorescence polarization applications is the competitive immunoassay used for the detection of therapeutic and illicit drugs. The method of fluorescence polarization has been used for clinical immunoassays for more than a decade. The homogeneous FPIA (fluorescence polarization in immunoassays) has well-accepted advantages over conventional heterogeneous immunoassays like RIA or ELISA. However, it fails if multi-binding step reactions are to be investigated because the separation of individually polarized species is impossible. Therefore, ligand binding curves only demonstrate the overall decrease of polarization, meaning the mechanistic binding constants cannot be determined. Further limitations are seen in sample volume as well as in mass restrictions.

With a two-dimensional fluorescence intensity distribution analysis according to the present invention, the full content of information usually buried in fluorescence anisotropy can be utilized, thereby overcoming the limitations mentioned above. 2D-FIDA directly determines two specific quantities per each fluorescence species in one measurement: the fluorescence intensity per molecule and the anisotropy of a given model. Based on this supplementary information, the delineation of all participating species and even the quantification of the binding behavior is possible. 2D-FIDA anisotropy is an ideal tool for the quantitative description of systems exhibiting multiple binding steps, aggregation and multimerization phenomena.

Theophylline therapy has been a cornerstone of asthma therapy for several years and, therefore, there is a strong demand for assaying and fine-tuning the theophylline level in serum. To demonstrate the capabilities of the present invention, the binding of theophylline antigens to anti-theophylline antibodies from a polyclonal anti-theophylline serum has been investigated. The antigens were labeled with 5'-carboxytetramethylrhodamine (TAMRA) with and without an incorporated spacer. In classical FP analysis these conjugates exhibited low anisotropy values (0.037 and 0.055 respectively) upon interacting with the antibody. Therefore they form a critical basis for illustrating the sensitivity of the present invention.

For the binding experiments the stock solutions of antibody and antigens were diluted in a PBS buffer with 0.05% Tween 20. After mixing the compounds, the mixture was incubated for 30 minutes at room temperature. Matching the spectral properties of the conjugates the system was excited at the 543 nm line of a He/Ne laser (Uniphase). As two examples, measured joint distributions of photon count numbers and results of 2D-FIDA applied to samples at different antibody dilution values but a constant ligand concentration of $[L] = 2nM$ are illustrated by **Figures 15** and **16**. Antibody concentrations are in arbitrary units referring to effective dilutions. Water background was below 1 kHz in each detection channel.

In the two-color fluorescence intensity distribution analysis according to the present invention, two detectors are spectrally tuned to monitor fluorescence from two labels of different color. In the assay type described below, ligand molecules are labeled in "green". Since each vesicle carries a high number of receptors, vesicles in samples with a low binding degree can be distinguished from vesicles in samples with high binding degree by a significantly higher specific brightness in "green". Vesicles are additionally stained in "red". Specific brightness of vesicles in "red" is not altered by binding of ligand molecules, but staining in "red" is a

means to increase contrast between free ligand molecules (which are nearly invisible in "red") and vesicles (which in the case of extremely low binding may be of nearly the same brightness in "green" as free ligand molecules). Contributions from the two fluorescent species of a single sample to the measured 2-dimensional distribution of the numbers of photon counts are very different in this assay type indeed, and therefore the analysis is highly reliable.

To demonstrate the advantages of a two-dimensional fluorescence intensity distribution analysis according to the present invention, the binding of TAMRA-labeled somatostatin-14 (SMS14-5TAMRA) to the human type-2 high affinity somatostatin receptor SSTR-2 (P. Schoeffter et al., Eur. J. Pharm., 289, 163 – 173, 1995) has been chosen as biological system. The receptor was expressed by CCL39hsst2 cells. Vesicles were prepared from this cell line and stained by the lipophilic tracer $DiC_{18}(5)$. The binding reaction was carried out in 10 mM HEPES (pH 7.6), 5 mM $MgCl_2$, 0.01% (w/v) fluorosurfactant FC-135, 1.33% DMSO in the presence of protease inhibitors. A schematical drawing of the principle of the assay is shown in **Figure 17**.

For excitation of fluorescence of the two spectrally distinct labels, the 532 nm line of a Neodym:Yag laser attenuated to 250 μW and the 632 nm line of a He-Ne laser attenuated to 25 μW were simultaneously used. In order to minimize misalignment of the two laser beams, they both passed through a single optical fiber before being focussed by the microscope. Also, the collected fluorescence beam passed a single pinhole before being splitted for the two detectors. An optical band-pass filter with the center wavelength 590 nm, FWHM 60 nm, and another one with the center wavelength 690 nm, FWHM 40 nm were used in front of the two detectors, monitoring fluorescence from the two labels separately. Because vesicles are slowly diffusing particles, in this experiment an area of 0,05 mm^2 of each sample was scanned, using

sinusoidal beam scanning of 25 Hz frequency, 100 µm amplitude in one direction, and sample scanning of 500 µm per 8 s data collection time in the other direction.

In **Figure 18** two typical examples of count number distributions corresponding to a high and a low degree of binding are compared. In **Figure 18 B**, the vesicle bound ligand (SMS14-5TAMRA) was competed off by the addition of a large excess of non fluorescent competitor (SRIF-14, SIGMA; 1 µM competitor, 3 nM total ligand). It is clearly visible that the distribution obtained in the absence of competitor (**Figure 18 A**) is more expanded in the n_2 direction than in the presence of competitor. The n_2 direction represents the green fluorescence of the labeled ligand and, hence, is a measure for the ligand binding.

2D-FIDA according to the present invention was applied to each of the measured distributions. Using a two-component fit algorithm, both the concentration (particle number in the confocal volume) and the fluorecence brightness values for the free ligand and the ligand bound to vesicles were obtained. The vesicles are well separated from the free ligand even in the presence of competitor (low binding). Addition of competitor leads to a decrease in the green fluorescence of the vesicles and an increase in the concentration of free ligand. The fact that the ligand does not completely dissociate from the vesicles is due to unspecific binding which is dependent on the amount of vesicles used in the assay.

Next, the competitor has been titrated from 1 µM down to 10 pM (10 measurements each) in order to record a dose-response curve and to determine the EC_{50} value. As shown in **Figure 19**, 2D-FIDA analysis leads to a typical sigmoidal competition curve with very low standard deviations. The calculated EC_{50} value is 0.87 nM which is in good agreement with EC_{50} values obtained using other evaluation methods (data not shown). Thus, it is not only possible to

differentiate between high and low binding but also small changes in the binding degree can be resolved with 2D-FIDA analysis according to the present invention. This is in particular important if one aims at the identification of assay inhibitors ("hits") in high throughput screening. In summary, 2D-FIDA analysis is a well-suited and highly reliable method for vesicle-based binding assays and has already been successfully applied in high throughput screening.

Reference is now made to **Figure 20**. According to a preferred embodiment, numbers of photon counts $\{\mathbf{n}_i\}$ subject to determination of a distribution function $\vec{P}(\mathbf{n})$ in step b) are derived from numbers of photon counts in primary time intervals $\{\mathbf{N}_j\}$ by addition of numbers of photon counts from primary time intervals according to a predetermined rule. One might e.g. be interested in choosing numbers of photon counts $\{\mathbf{n}_i\}$ subject to determination of a distribution function $\vec{P}(\mathbf{n})$ which are calculated from the numbers of photon counts in primary time intervals $\{\mathbf{N}_j\}$ according to the rule $\mathbf{n}_i = \sum_{k=1}^{M} \mathbf{N}_{Mi+k}$, where M is an integer number expressing how many times the time interval in which $\{\mathbf{n}_i\}$ is determined is longer than the primary time interval. Line N shows the primary time interval windows. Line $\mathbf{n}_i$ indicates the primary time windows chosen to calculate $\mathbf{n}_i$ according to the rule.

Figure 21 shows a further embodiment in which numbers of photon counts $\{\mathbf{n}_i\}$ are derived from predetermined primary time intervals according to a rule in which primary time intervals are separated by a time delay. In particular, the following rule can be applied: $\mathbf{n}_i = \sum_{k=1}^{M} (\mathbf{N}_{Mi-k} + \mathbf{N}_{M(i+L)+k})$, where M and L are positive integer numbers, $\{\mathbf{n}_i\}$ are numbers of photon counts subject to determination of a distribution function $\vec{P}(\mathbf{n})$, and $\{\mathbf{N}_j\}$ are the numbers of photon counts in primary time intervals.

Reference is now made to **figures 22 to 27**.

The study of function and activity of cell surface receptors is central to all disciplines of modern biology and pharmacology. Membrane receptors play a key role in communication within a multicellular organism since they transduce extracellular signals across the plasma

membrane into the cell. Two important classes of membrane receptors are growth factor receptors and G protein-coupled receptors (GPCR). Growth factor receptors belong to the family of receptor tyrosine kinases which play an important role in cell differentiation and growth. Receptors belonging to this class include the epidermal growth factor receptor family, the neurotrophin receptor family and insulin receptors (Mc Innes C. & Sykes B.D. Biopolymers, 43, 339 – 366, 1997; Riese D.J. & Stern D. F., Bioessays 20, 41 – 48, 1998; Persson H. & Ibanez C.F., Curr. Opin. Neurol. Neurosurg. 6, 11 – 18, 1993). G protein-coupled receptors are a superfamily of integral membrane proteins containing seven α-helical transmembrane domains which mediate transmembrane signal transduction of a variety of processes by binding extracellular factors such as neurotransmitters and hormones (Ji et al., J. Biol.Chem., 273, 17299 – 17302, 1998; Gether et al., J. Biol. Chem. 273, 17979 – 17982, 1998; Wess J., FASEB J. 11, 346 – 354, 1997).

In most cases, receptors are studied biochemically and pharmacologically using radioligand binding assays. In these experiments, binding of radioactively labeled ligands to membrane fractions or to whole cells is monitored, frequently involving separation of bound and free ligand. Using the method according to the present invention, the characterization of fluorescently-labeled molecules or particles with respect to their molecular brightness and concentration at the single molecule level is possible. In the following it is described how this method can be applied to study ligand-receptor interactions. Bound ligand can be distinguished from unbound ligand due to the accumulation of fluorescent ligand molecules on receptor-bearing vesicles, resulting in an increased particle brightness compared to single fluorescent ligand molecules. With fluorescence intensity distribution analysis (FIDA) according to the present invention, these differences in molecular brightness can be quantified and the absolute concentrations of free and bound ligand are determined in a single measurement without the need for separation. Since FIDA takes advantage of a highly focused laser beam the detection volume is roughly the size of 1 femtoliter. The sample volumes can be reduced to 1 µl which currently is the practical limit of liquid handling, thus offering significant savings of precious biological material and chemical compounds. The results demonstrate that FIDA is an ideal method for receptor-ligand studies offering substantial benefits for research and high-throughput pharmaceutical screening: it is widely applicable, circumvents the use of hazardous and expensive radioactive probes, overcomes the need for

washing steps (i.e. the present invention provides a homogeneous assay method) and enables significant reduction in reagent consumption.

Both classes of receptors described above play an important role in a large number of diseases such as cancer, neurodegenerative diseases, cardiovascular disorders and AIDS and are thus important drug targets. The EGF receptor (EGFR/ErbB1), a 170 kD receptor tyrosine kinase and the β2- adrenergic receptor, a G protein-coupled receptor as our model systems.

The following experimental protocol has been used:

Materials. Tetramethylrhodamine labelled epidermal growth factor (TMR-EGF), unlabeled epidermal growth factor (EGF) and Bodipy FL-CGP 12177 (Bodipy FL: 4,4-difluoro-5,7-dimethyl-4-bora-3a,4a-diaza-s-indacene-3-propionic acid; CGP 12177: 4-[3-[(1,1-Dimethylethyl)amino]-2-hydroxypropoxy]-1,3-dihydro-2H-benzimidazol-2-one hydrochloride) were purchased from Molecular Probes (Leiden, Netherlands). Human epidermoid carcinoma (A431) cells and human colon carcinoma tumor (HCT) cells were obtained from the American Type Tissue Culture Collection. Betacellulin and heparin-binding EGF (HB-EGF) were purchased from R & D Systems and CGP 12177A from RBI (Natick, USA).

Methods. Cell lines and membrane preparations. Wild type human β2 adrenergic receptor cDNA was cloned into the plasmid pcDNA3. The plasmid was transfected into HEK293 cells and stable clones were selected as described (Gabilondo A.M., Hegler J., Krasel C., Boivin-Jahns V., Hein L., Lohse M. J., Proc. Natl. Acad. Sci. U.S.A., 94, 12285 – 12290, 1997). For membrane preparations, approximately 2×10^8 cells were resuspended in 2 ml of ice cold lysis buffer (10 mM Tris-HCl pH 7.4, 1 mM $MgSO_4$, 0.5 mM EDTA containing a protease inhibitor cocktail (Complete™ Mini EDTA-free, Roche Molecular Biochemicals). Cells were disrupted by Dounce homogenization on ice and unbroken cells and nuclei were removed by centrifugation at 900 x g for 10 min. The supernatants were pooled and centrifuged at 100,000 x g for 20 min (4°C). Membrane pellets were resuspended in 0.5 ml binding assay buffer and the protein concentration was determined using a Bradford protein assay (Biorad). Membranes were frozen in aliquots in liquid nitrogen and stored at -80°C.

Binding studies. Typical experiments contained 50 to 500 µg/ml of membrane protein, different concentrations of fluorescent ligand and competitor in a final volume of 40 µl (see Figure legends for details). EGF receptor (EGFR) binding studies were carried out in 20 mM

Hepes pH 7 4, 140 mM NaCl, 5 mM KCl, 1.2 mM $MgCl_2$, 1.8 mM $CaCl_2$, 0.1% BSA and 0.1% CHAPS. The binding assay buffer for the β2 adrenergic receptor contained 75 mM Tris-HCl pH 7.4, 10 mM $MgCl_2$, 2 mM EDTA, 0.05% BSA and 0.1% CHAPS. Measurements were carried out in 8 well glass chambers (Nunc). For experiments with sample volumes of 1 µl, proprietary liquid dispensing units and high-density sample carriers (Nanocarrier) with a total capacity of 1.5 µl per well were used (EVOTEC BioSystems AG).

Data analysis. A confocal microscope was used (Confocor, EVOTEC BioSystems AG and Carl Zeiss Jena, Germany) with an optical set-up described in Kask P., Palo K., Ullmann D. & Gall K. (Proc. Natl. Acad. Sci. U.S.A., 96, 13756 – 13761, 1999; the contents of which are herein incorporated by reference). The number of photon counts was measured at 40 µs dwell time with a data collection time of 4 - 8 s per well. Measurements with TMR-EGF were carried out at excitation/emission wavelengths of 543/580 nm using a helium/neon laser attenuated to approximately 300 µW. Measurements with Bodipy FL-CGP 12177 were carried out at excitation/emission wavelengths of 488/520 nm using an $Argon^+$ laser attenuated to approximately 2 mW. Like FCS, the method according to the present invention relies on the random diffusion of fluorescent particles in and out of the confocal volume (Kask P., Palo K., Ullmann D. & Gall K., Proc. Natl. Acad. Sci. U.S.A., 96, 13756 – 13761, 1999; Rigler R., J. Biotechnol. 41, 177 – 186, 1995). Since the diffusion time of membrane particles is very high compared to single molecules such as proteins (mean diffusion time τ = 10 –100 ms versus approximately 200 µs – 1 ms for single molecules), advantage was taken of a two-dimensional scanning approach in order to be able to detect sufficiently large numbers of fluorescent membraneous vesicles. This is achieved using a laser beam oscillator and a mobile sample stage.

Assuming the presence of two different fluorescent species within the sample, namely fluorescent ligand and vesicles with fluorescent ligand accumulated on their surface, the photon distribution was fit with the multicomponent fit according to Kask P., Palo K., Ullmann D. & Gall K.(Proc. Natl. Acad. Sci. U.S.A., 96, 13756 – 13761, 1999; the contents of which are herein incorporated by reference) in order to determine molecular brightnesses and absolute concentrations of these two components. Concentrations of bound and free ligand were deduced from that data. The amount of ligand bound to vesicles is given either in concentrations (nM ligand bound) or as fractional binding (ligand bound divided by ligand total). Apparent affinities (K_i) were calculated from the concentration giving half-maximal displacement (IC_{50}, obtained by non-linear l ast-squares curve-fitting to a one-site binding

model), using the relationship $K_I = IC_{50}/(1 + (\text{ligand concentration} / K_D))$ according to Cheng Y. & Prusoff W. H. (Biochem. Pharmacol. 22, 3099 – 3108, 1973). Experimental data were analyzed using Prism 3.0 (Graph Pad Prism, San Diego, USA).

Fluorescence intensity distribution analysis (FIDA) allows the study of molecular interactions of fluorescent molecules if a change of particle brightness occurs upon binding. Quantitative data describing molecular interactions are obtained since the molecular brightness of each fluorescent species in the sample and their respective absolute concentrations are determined. **Figure 22** shows a schematic diagram of binding of a fluorescently-labeled molecule to receptor-bearing vesicles as observed by the method according to the present invention. The confocal volume is represented by the central black square. **A**: In the absence of membranes, the confocal volume contains exclusively free fluorescent ligand molecules. The molecular brightness of the fluorescent ligand is an intrinsic property of the fluorophore and the molecule it is attached to. **B**: A brightness distribution obtained for the sample shown in A with a typical molecular brightness for free ligand of 7 kHz. **C**: After the addition of vesicles, ligand binding occurs and the confocal volume is populated with both vesicle-bound and free ligand. **D**: Brightness distribution of sample shown in C. The molecular brightness of unbound ligand remains 7 kHz. The molecular brightness of vesicles was 98 kHz in this case (14 times the brightness of free ligand, corresponding to 14 ligand molecules bound per vesicle) and depends on the receptor expression level. Typically, 10 – 500 ligand molecules per vesicle can be found. Note: sizes are not to scale. Thus, although the total fluorescence does not change upon binding, both the molar concentration of bound as well as the molar concentrations of unbound ligand are quantitatively determined from a single measurement without any separation being necessary.

The method according to the present invention has been used to characterize the interaction of TMR-labeled EGF with its receptor, the EGF receptor (EGFR/ErbB1). As a source, A431 cells were used which are known to overexpress EGFR (Mc Culloch et al., Int. J. Biochem. Cell Biol. 30, 1265 – 1278, 1998). **Figure 23** shows the ligand binding characteristics of TMR-EGF to membranes prepared from A431 cells. Ligand concentrations from 0.25 – 18 nM were incubated with a crude membrane fraction at a final concentration of 50 µg/ml in a total volume of 40 µl. After an incubation period of 20 min at room temperature, measurements were carried out, and free and bound ligand concentrations determined.

Binding of TMR-labeled EGF to the membranes is saturable and can be competed by an excess of unlabelled EGF. Non-specific binding was determined in the presence of 1 μM EGF. The results shown are from a typical experiments, the standard deviation (SD) is shown as error bars. The determined dissociation constant (K_D) of 3.1 ± 0.2 nM is consistent with earlier reports where fluorescently-labelled EGF was used as a competitor in radio-ligand binding assays (Carraway et al. J. Biol. Chem. 266, 8899-8906, 1991). An expression level (B_{max}) of 60 pmol/mg was observed which corresponds to approximately 6x 10^6 binding sites per cell, indicating that the level of expression of EGFR in A431 is upregulated significantly as confirmed by earlier reports (Mc Culloch et al., Int. J. Biochem. Cell Biol. 30, 1265-1278, 1998).

In order to demonstrate that the method according to the present invention is also applicable to biological systems with much lower, more physiological expression levels, human colon carcinoma tumor (HCT) cells were used. **Figure 24** shows the TMR-EGF binding to membranes prepared from HCT cells. Increasing amounts of crude membranes prepared from HCT cells were incubated with 2 nM TMR-EGF in the presence and absence of unlabeled EGF. Total and non-specific binding was determined by the method according to the present invention. Ligand bound is expressed as fractional binding (ligand bound divided by ligand total). Membranes prepared from HCT cells bind TMR-EGF, where specific binding was 70 – 80 % of total binding. The affinity and expression levels were determined in a saturation curve as shown for A431 cells in Figure 23 (data not shown). The K_D was found to be 3 nM which is very similar to the affinity of the EGF receptor in A431 cells (see Figure 23). The B_{max} was found to be 400 fmol / mg membrane protein which corresponds to approximately 10,000 – 20,000 binding sites / cell and is thus more than 100 times lower than in A431 cells. This experiment demonstrates that FIDA can not only be used with receptor-overexpressing cell lines but also with receptor densities equivalent to those in their natural environment.

Since the EGF receptor is part of a family of related receptor tyrosine kinases which bind different growth factors (EGFR/ErbB-1, ErbB-2, Erb-B3 and ErbB-4; Riese et al. Bioessays 20, 41 – 48, 1998) the interaction of TMR-EGF with HCT membranes has been further characterized. The number of mammalian polypeptide growth factors exhibiting significant sequence identity with EGF has increased dramatically in recent years and include betacellulin and heparin-binding EGF (HB-EGF). **Figure 25** illustrates the pharmacological profile of the

EGF receptor. The affinity of unlabelled EGF, betacellulin and heparin-binding epidermal growth factor (HB-EGF) was determined by competition assays incubating HCT membranes with TMR-EGF and the indicated concentrations of competitor. Binding was determined by the method according to the present invention and was normalized to that in the absence of competitor. The affinities obtained were 0.35 ± 0.12 nM for EGF, 0.23 ± 0.02 nM for betacellulin and 1.4 ± 0.3 nM for HB-EGF.

As a further system, the β2 adrenergic receptor was used since it is a well known model system for the large family of G protein-coupled receptors (Kobilka, Annu. Rev. Neurosci. 1587 – 114, 1992). Fluorescently-labeled CGP 12177, a β2 adrenergic receptor antagonist, was chosen as a ligand (Heithier et al., Biochemistry 33, 9126 – 9134, 1994). **Figure 26** illustrates the ligand binding characteristics of Bodipy FL-CGP 12177. Increasing concentrations of Bodipy FL-CGP 12177 were incubated with a crude membrane fraction derived from HEK 293 cells expressing the human β2 adrenergic receptor. The final membrane concentration was 130 µg/ml in a total volume of 40 µl. Non-specific binding was determined in the presence of 1 µM propranolol and was subtracted from total binding. The results shown are from a typical experiments, standard deviations (SD) are shown as error bars. Bodipy FL-CGP 12177 bound to an apparently homogenous population of binding sites. Binding of the ligand was statistically best fit using a single site model with a mean affinity of 0.7 nM, which is similar to the results obtained when using standard filter binding assays (Heithier et al., Biochemistry 33, 9126 – 9134, 1994), and a B_{max} of 4 pmol/mg. Competition experiments with unlabelled CGP 12177 yielded a K_i of 0.8 nM, indicating that the attachment of the fluorescent label does not affect the affinity for the receptor significantly.

Figure 27 illustrates the inhibition of Bodipy FL-CGP 12177 binding in 40 µl and 1 µl assay volumes. Unlabelled ligand (CGP 12177A) was used as a competitor at the concentrations shown. Binding was normalized to 100% at maximal binding. The binding assay was carried out in sample volumes of 40 µl and 1 µl. For experiments involving sample volumes of 1 µl, proprietary liquid dispensing units and sample carriers were used (EVOTEC BioSystems AG). The affinities obtained for CGP12177 were 0.7 ± 0.1 nM in 40 µl and 0.9 ± 0.1 in 1 µl assay volumes. This experiment emphasizes the unique sensitivity of FIDA and poses a large opportunity for a significant reduction of sample volumes and thus of the required biological material for high-throughput drug screening.

Studying ligand-receptor interactions is an important tool for the biological and pharmacological characterization of membrane receptor function. Particularly, G protein-coupled receptors are of high interest for pharmaceutical drug discovery programs since approximately 30 - 50% of all drugs on the market today are estimated to act on GPCR (Gudermann et al. J. Mol. Med. 73, 51 – 63, 1995). Traditionally, the majority of ligand-receptor studies are carried out using radioactively-labeled ligands, where bound from unbound ligand is separated by either filtration or centrifugation. In recent years, scintillation proximity assays have found widespread use for receptor-ligand binding studies. Here, binding events are detected by the proximity of the radioligand to membranes immobilized on a scintillant-containing bead, thus eliminating the need for separation (Hart, Mol. Immunol. 16, 265 – 267, 1979). However, the disadvantages of these methods are potentially hazardous exposure to radioactive compounds, limited shelf half-life of labeled ligands and special requirements for handling and disposal of reagents. Therefore, a number of fluorescence-based detection methods have been applied to receptor-ligand studies in recent years which are based on the detection of total fluorescence (Heithier et al, Biochemistry 33, 9126 – 9134, 1994; Inglese et al. Biochemistry 37, 2372 – 2377, 1998), fluorescence quenching / spectral shift (Tairi et al., Biochemistry 37, 15850 – 15864, 1998), fluorescence polarization (Tairi et al., Biochemistry 37, 15850 – 15864, 1998) or on the use of laser-scanning imaging (Zuck et al. Proc. Natl. Acad. Sci. USA, 11122 – 1127, 1999).

Based on the method according to the present invention, fluorescence intensity distribution analysis can be used to characterize quantitatively the interaction of ligands with their cognate receptors. Since FIDA allows interactions to be studied with single molecule sensitivity, it offers significant advantages over the methods described above. Using EGF and β2 adrenergic receptors as model systems it has been shown in the examples above that affinities and receptor expression levels can be quantitated in a simple manner. The results demonstrate that the pharmacological profiles obtained using FIDA correspond to those obtained by classical radioligand binding assays. It has also been shown that FIDA can be used to study ligand-receptor interactions using cells expressing low levels of receptor. This is of particular importance for GPCRs since they are typically found in low density in primary tissues and overexpression of functional receptors is often difficult to achieve. Since FIDA allows to quantitate the increase in particle brightness upon binding of multiple fluorescent molecules to

vesicles, no changes of fluorescence parameters such as fluorescence quenching or spectral shift are required to occur, making this approach widely applicable. With FIDA, molar concentrations of both free and bound ligand are determined in a single measurement thus providing an internal control as to how much total ligand is present in each sample. A significant advantage of FIDA is the small volume of detection, which is approximately the size of a bacterial cell. Miniaturization of assay volumes is a key strategy in modern pharmaceutical drug screening since increasing numbers of chemical compounds have to be screened against a growing number of biological targets, consumption of biological reagents and of chemical or natural compounds therefore becomes a major issue. FIDA and related preferably confocal methods based on the present invention are therefore ideally suited for these purposes since the sample volume can be reduced to 1 µl, which is the current limit of liquid handling, without compromising the signal-to-noise ratio, therefore offering unique sensitivity.

FIDA has been successfully appied to study a number of different types of G protein-coupled receptors in our laboratory. These include chemokine receptors, dopamine receptors and a number of peptide receptors. These assay systems include the usage of small labeled molecules (agonists or antagonists such as described in this study), peptides and proteins (data not shown). In addition, the technology can be successfully applied to measure binding of molecules to live cells in a 1 µl format. This opens the exciting opportunity of using primary tissues directly in high-throughput screening.

In conclusion, FIDA is an ideal method for ligand-receptor studies: It offers significant advantages for research, high-throughput screening and for pharmacological profiling since it circumvents the use of radioactive isotopes and of separation steps, is widely applicable and it allows a significant reduction of reagent consumption.

CLAIMS

1. A method for characterizing fluorescent molecules or other particles in samples comprising the steps of:

a) monitoring fluctuating intensity of fluorescence emitted by the molecules or other particles in at least one measurement volume of a non-uniform spatial brightness profile by measuring numbers of photon counts in primary time intervals by a single or more photon detectors,

b) determining at least one distribution function of numbers of photon counts, $\vec{P}(\mathbf{n})$, from the measured numbers of photon counts,

c) determining physical quantities characteristic to said particles by fitting the experimentally determined distribution function of numbers of photon counts,

wherein the fitting procedure involves calculation of a theoretical distribution function of the number of photon counts $P(\mathbf{n})$ through its generating function, defined as $G(\vec{\xi}) = \sum_{n} \vec{\xi}^{\mathbf{n}} P(\mathbf{n})$.

2. A method according to claim 1 wherein the primary time intervals are consecutive intervals of equal width.

3. A method according to one of claims 1 and 2 wherein in step b) numbers of photon counts $\{\mathbf{n}_i\}$ subject to determination of a distribution function $\vec{P}(\mathbf{n})$ are derived from numbers of photon counts in primary time intervals $\{\mathbf{N}_j\}$ by addition of numbers of photon counts from primary time intervals according to a predetermined rule.

4. A method according to claim 3 wherein in step b) numbers of photon counts $\{\mathbf{n}_i\}$ subject to determination of a distribution function $\vec{P}(\mathbf{n})$ are calculated from the numbers of photon counts in primary time intervals $\{\mathbf{N}_j\}$ according to the rule $\mathbf{n}_i = \sum_{k=1}^{M} \mathbf{N}_{Mi+k}$, where M is an integer number expressing how many times the time interval in which $\{\mathbf{n}_i\}$ is determined is longer than the primary time interval.

5. A method according to claim 3 wherein in step b) numbers of photon counts $\{n_i\}$ are calculated from predetermined primary time intervals according to a rule in which primary time intervals are separated by a time delay.

6. A method according to claim 5 wherein in step b) numbers of photon counts $\{n_i\}$ subject to determination of a distribution function $\vec{P}(\mathbf{n})$ are calculated from the numbers of photon counts in primary time intervals $\{N_j\}$ according to the rule $n_i = \sum_{k=1}^{M}(N_{Mi+k} + N_{M(i+L)+k})$, where M and L are positive integer numbers.

7. A method according to one of the claims 3 to 6 wherein in step b) a set of distribution functions $\vec{P}(\mathbf{n})$ is determined according to a set of different rules, said set of distribution functions being fitted jointly in step c).

8. A method according to claim 7 wherein in step c) a set of distribution functions with different values of M and/or L are fitted jointly.

9. A method according to one of the claims 1 to 8 wherein at least one of the physical quantities of step c) is concentration of particles.

10. A method according to one of the claims 1 to 9 wherein at least one of the physical quantities of step c) is specific brightness of particles.

11. A method according to one of the claims 1 to 10, wherein at least one of the physical quantities of step c) is diffusion coefficient.

12. A method according to one of the claims 1 to 11 wherein the generating function is calculated using the expression $G(\xi) = \exp[\int dq c(q) \int d^3\mathbf{r}(e^{(\xi-1)qTB(\mathbf{r})} - 1)]$, where $c(q)$ is the density of particles with specific brightness q, T is the length of the counting interval, and $B(\mathbf{r})$ is the spatial brightness profile as a function of coordinates.

13. A method according to one of the claims 1 to 12 wherein the argument of the generating function is selected in the form $\xi = e^{-i\varphi}$ and a fast Fourier transform algorithm is used in calculation of the theoretical distribution of the number of photon counts out of its generating function.

14. A method according to one of the claims 1 to 13 wherein in step c) when calculating the theoretical distribution $P(\mathbf{n})$, the spatial brightness profile is modelled by a mathematical relationship between volume and spatial brightness.

15. A method according to claim 14 wherein in step c) when calculating the theoretical distribution $P(\mathbf{n})$, the spatial brightness profile is modelled by the following expression: $\frac{dV}{dx} = a_1 x + a_2 x^2 + a_3 x^3$, where dV denotes a volume element, x denotes logarithm of the relative spatial brightness, and a_1, a_2 and a_3 are empirically estimated parameters.

16. A method according to any of the claims 1 to 15 wherein in step a) a confocal microscope is used for monitoring the intensity of fluorescence.

17. Use of a confocal apparatus for performing the method according to any of the claims 1 to 16 comprising:

a radiation source (12) for providing excitation radiation (14),

an objective (22) for focussing the excitation radiation (14) into a measurement volume (26),

a detector (42) for detecting emission radiation (30) that stems from the measurement volume (26), and

an opaque means (44) positioned in the pathway (32) of the emission radiation (30) or excitation radiation (14) for erasing the central part of the emission radiation (30) or excitation radiation (14).

ABSTRACT

A method for characterizing fluorescent molecules or other particles in samples comprising the steps of:

a) monitoring fluctuating intensity of fluorescence emitted by the molecules or other particles in at least one measurement volume of a non-uniform spatial brightness profile by measuring numbers of photon counts in primary time intervals by a single or more photon detectors,

b) determining at least one distribution function of numbers of photon counts, $\vec{P}(\mathbf{n})$, from the measured numbers of photon counts,

c) determining physical quantities characteristic to said particles by fitting the experimentally determined distribution function of numbers of photon counts,

wherein the fitting procedure involves calculation of a theoretical distribution function of the number of photon counts $P(\mathbf{n})$ through its generating function, defined as $G(\vec{\xi}) = \sum_{n} \vec{\xi}^{\mathbf{n}} P(\mathbf{n})$.

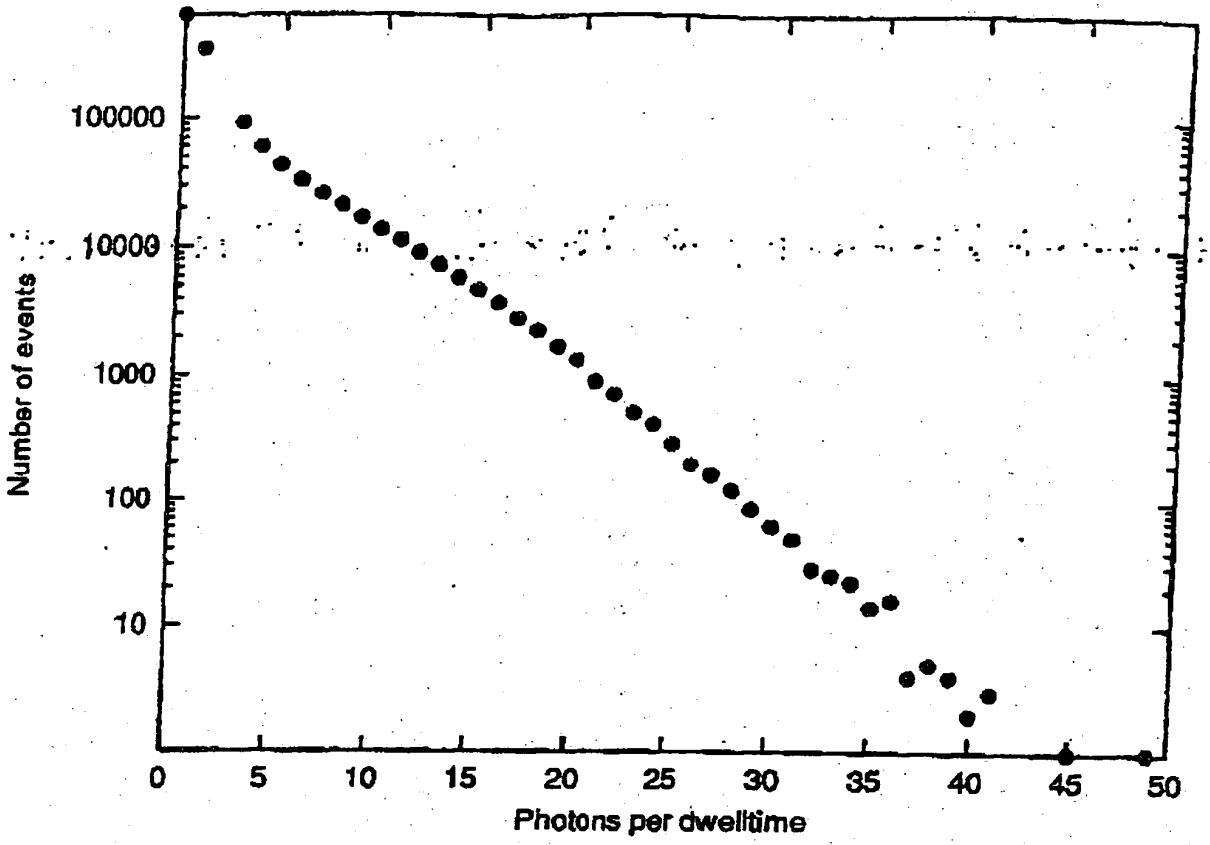
100000
10000
1000
100
10
Number of events
0
5
10
15
20
25
30
35
40
45
50
Photons per dwelltime

Fig. 1a

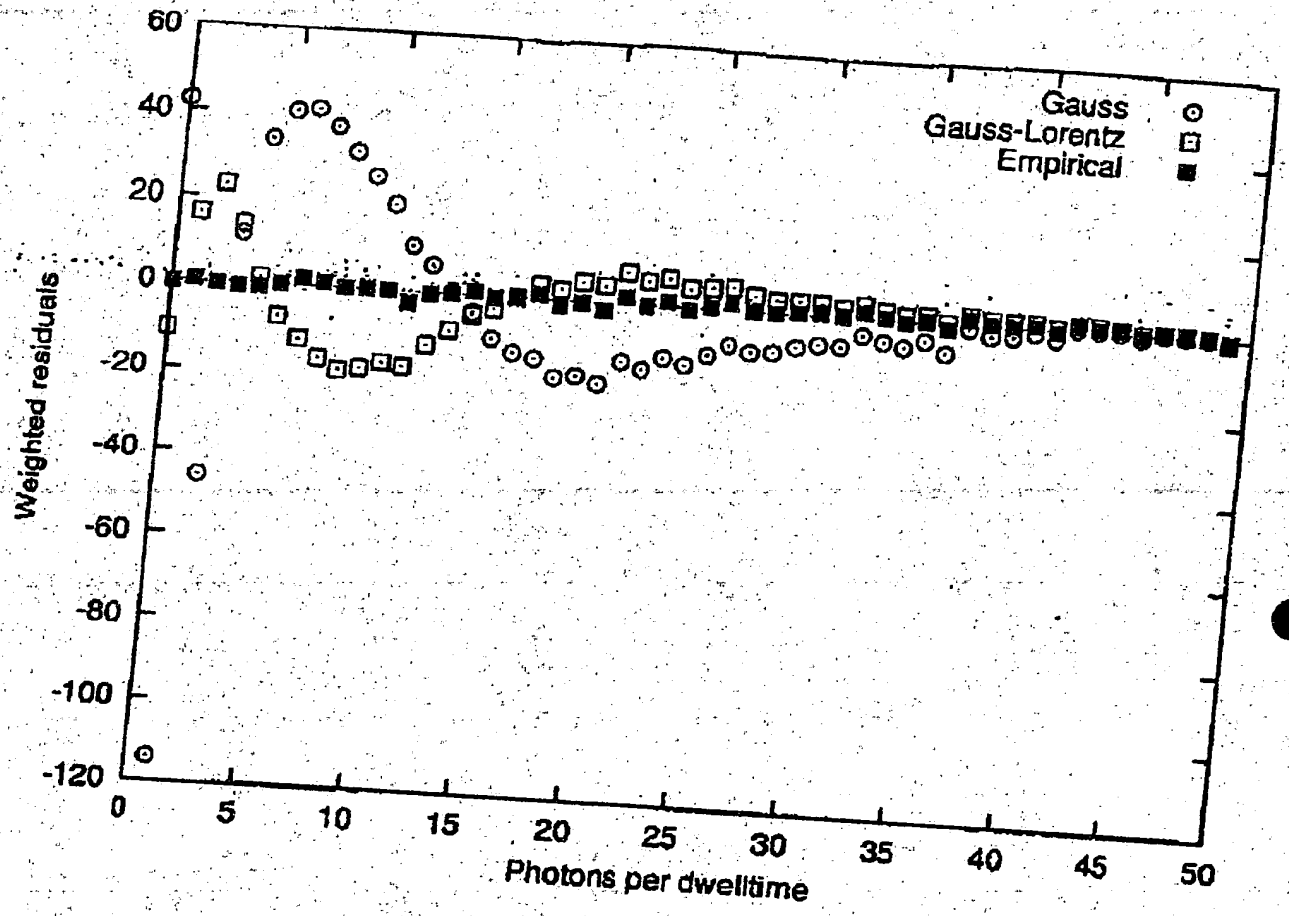
Gauss
Gauss-Lorentz
Empirical
Weighted residuals
60
40
20
0
-20
-40
-60
-80
-100
-120
0
5
10
15
20
25
30
35
40
45
50
Photons per dwelltime

Fig. 1b

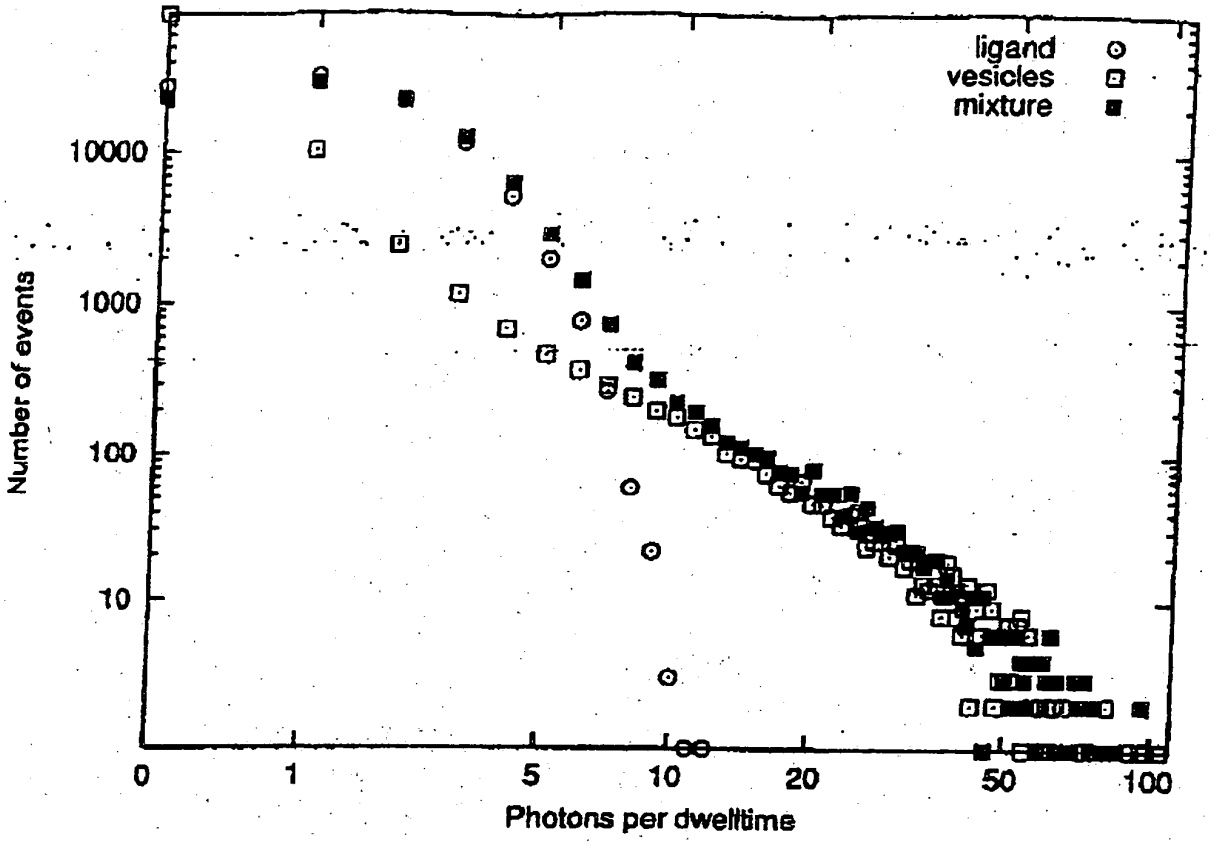
ligand
vesicles
mixture
Number of events
10000
1000
100
10
0
1
5
10
20
50
100
Photons per dwelltime

Fig. 2

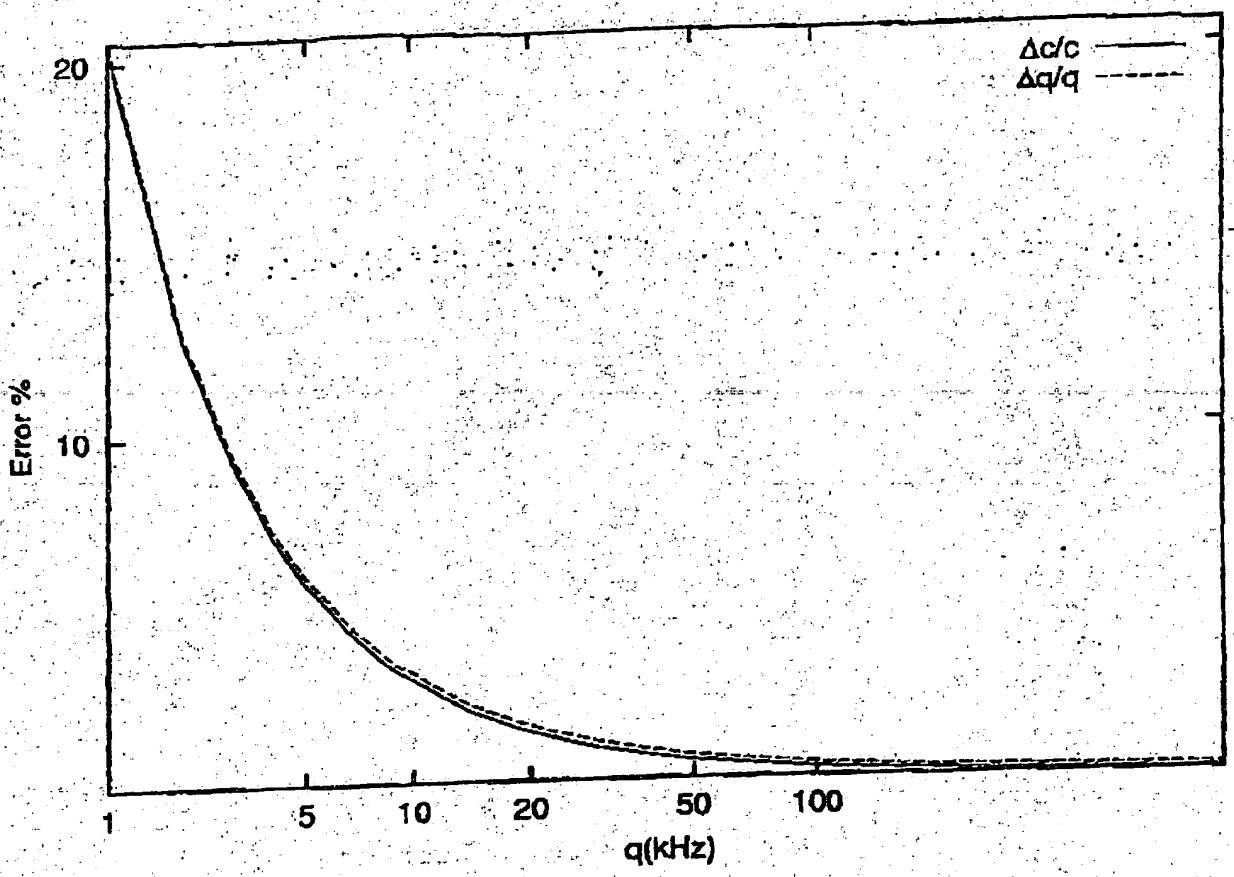

Fig. 3

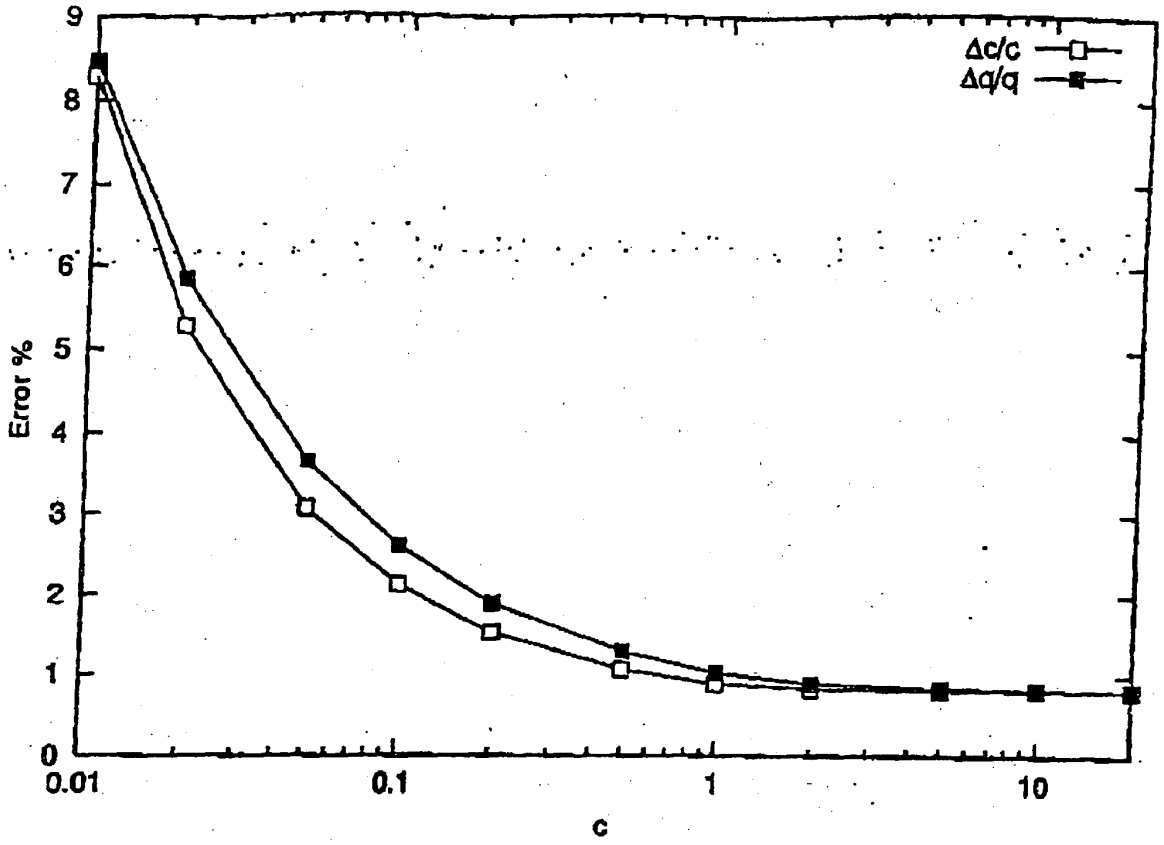

Fig. 4

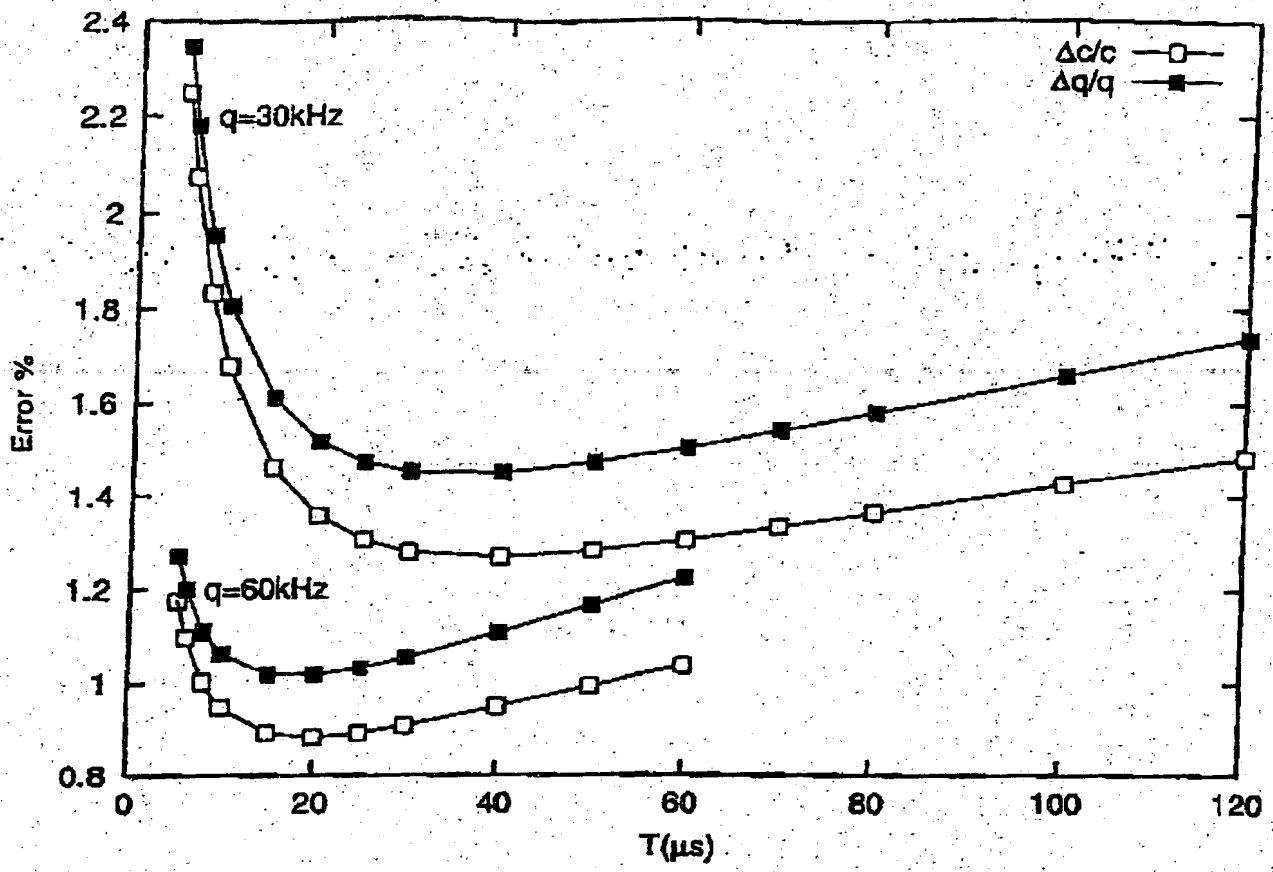
Δc/c
Δq/q
q=30kHz
q=60kHz
Error %
T(μs)
2.4
2.2
2
1.8
1.6
1.4
1.2
1
0.8
0
20
40
60
80
100
120

Fig. 5

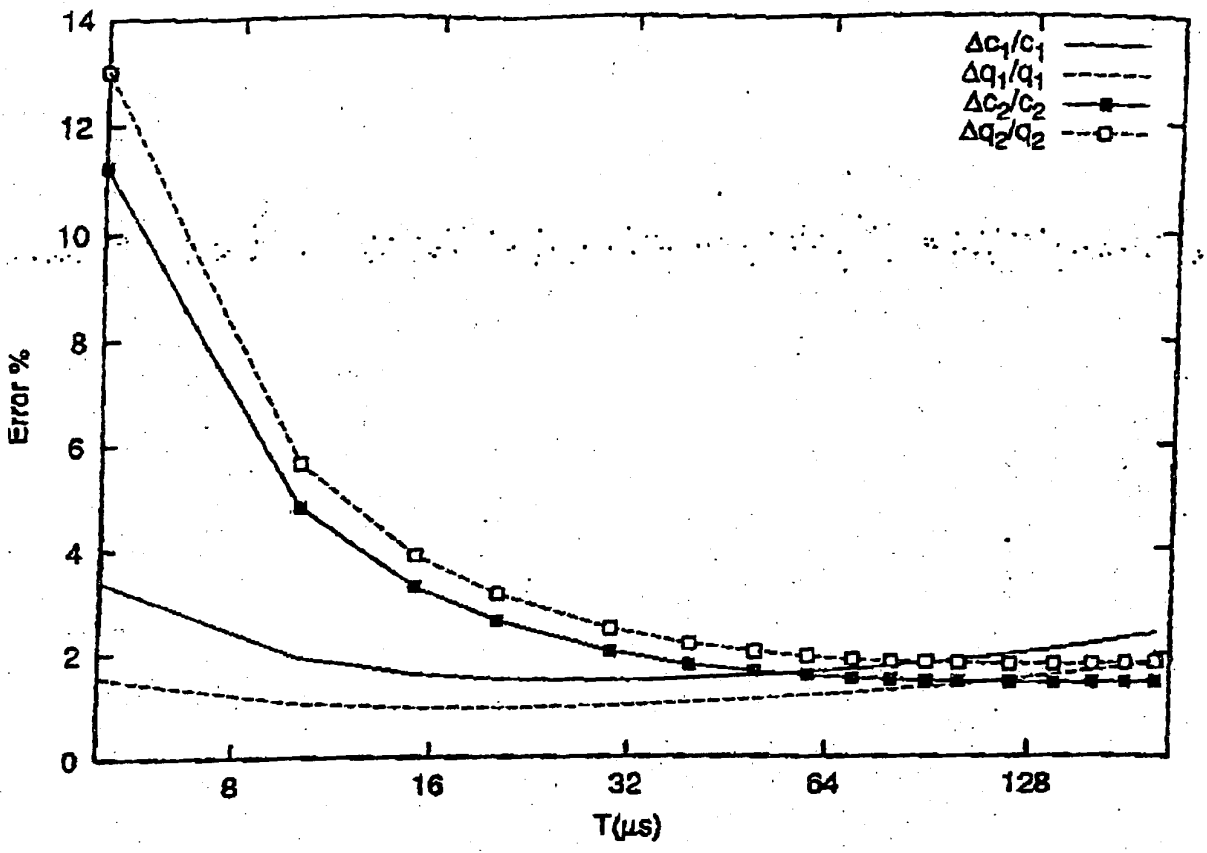

Fig. 6

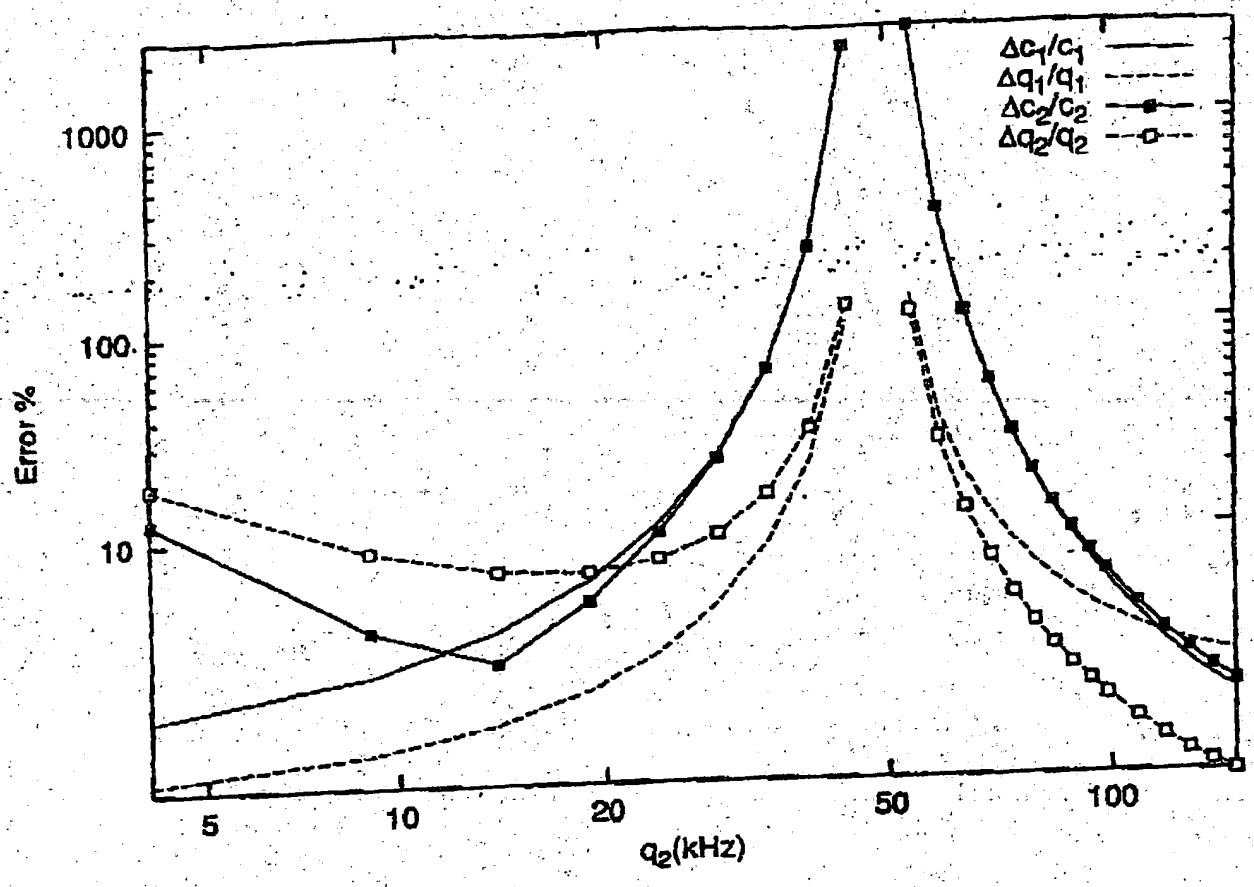
$\Delta c_1/c_1$
$\Delta q_1/q_1$
$\Delta c_2/c_2$
$\Delta q_2/q_2$
1000
100
10
Error %
5
10
20
50
100
q_2(kHz)

Fig. 7

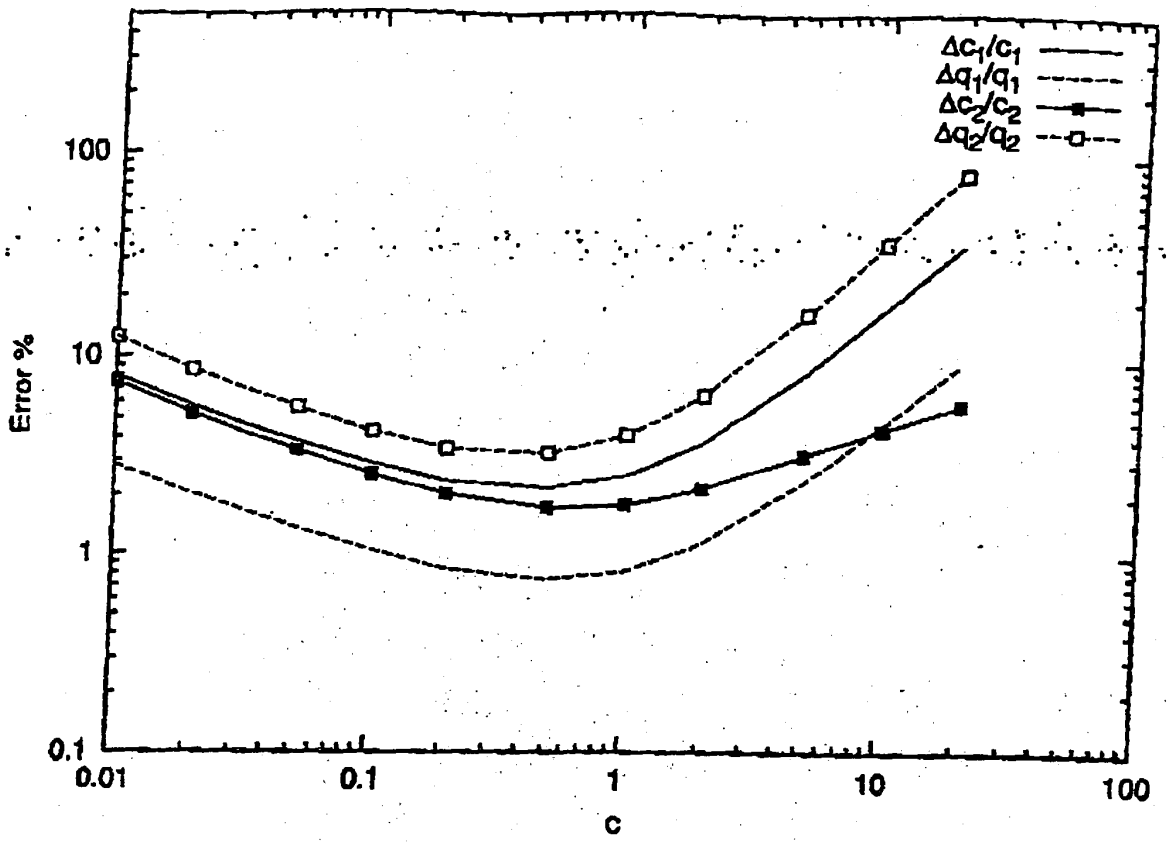
$\Delta c_1/c_1$
$\Delta q_1/q_1$
$\Delta c_2/c_2$
$\Delta q_2/q_2$
100
10
1
0.1
Error %
0.01
0.1
1
10
100
c

Fig. 8

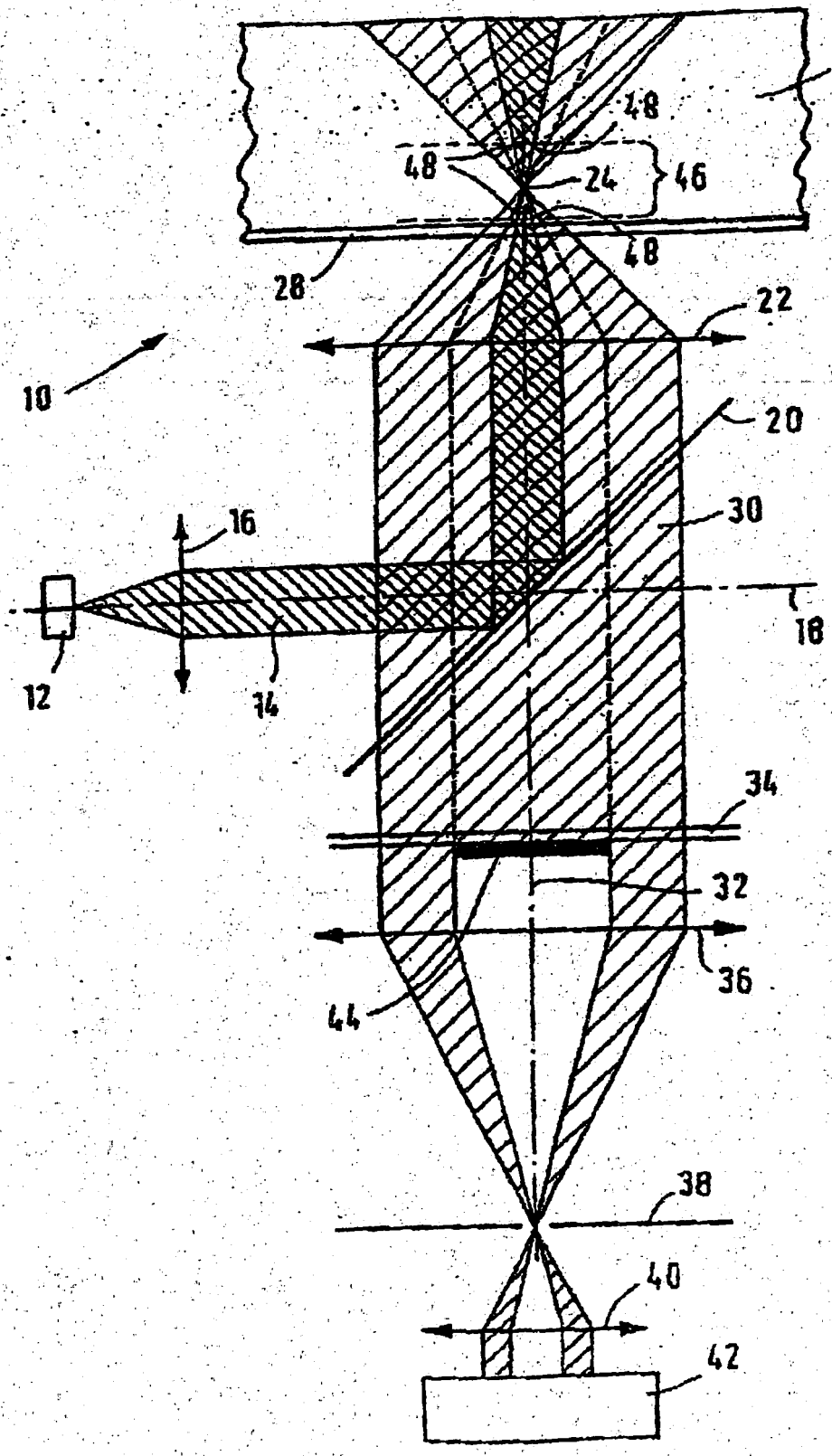

Figure 9

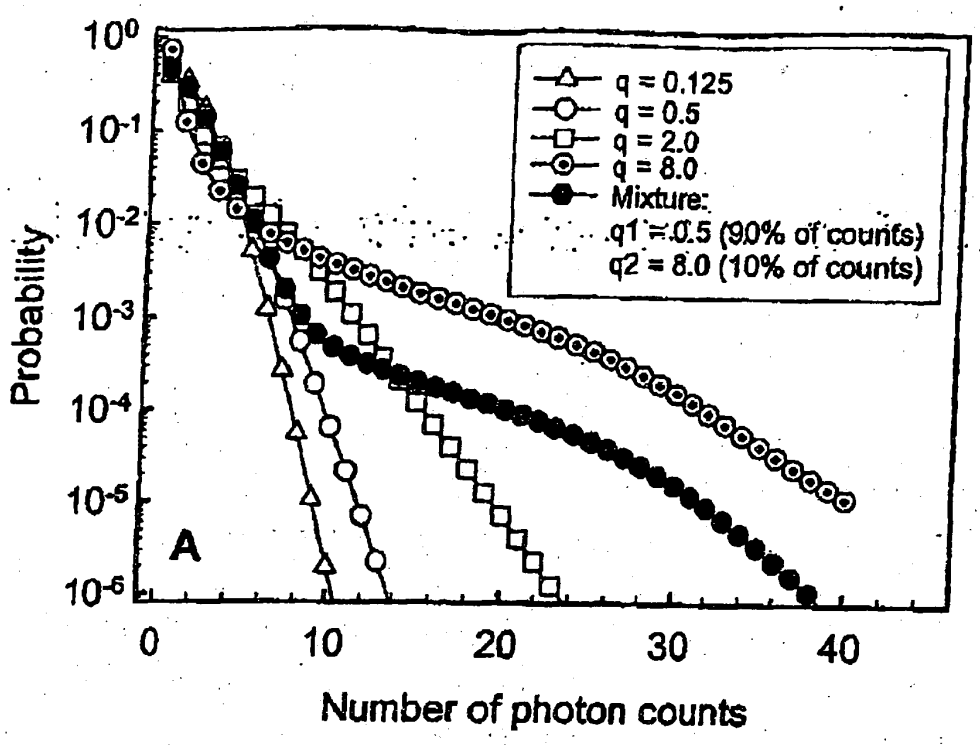
Probability
Number of photon counts
A
q = 0.125
q = 0.5
q = 2.0
q = 8.0
Mixture:
q1 = 0.5 (90% of counts)
q2 = 8.0 (10% of counts)

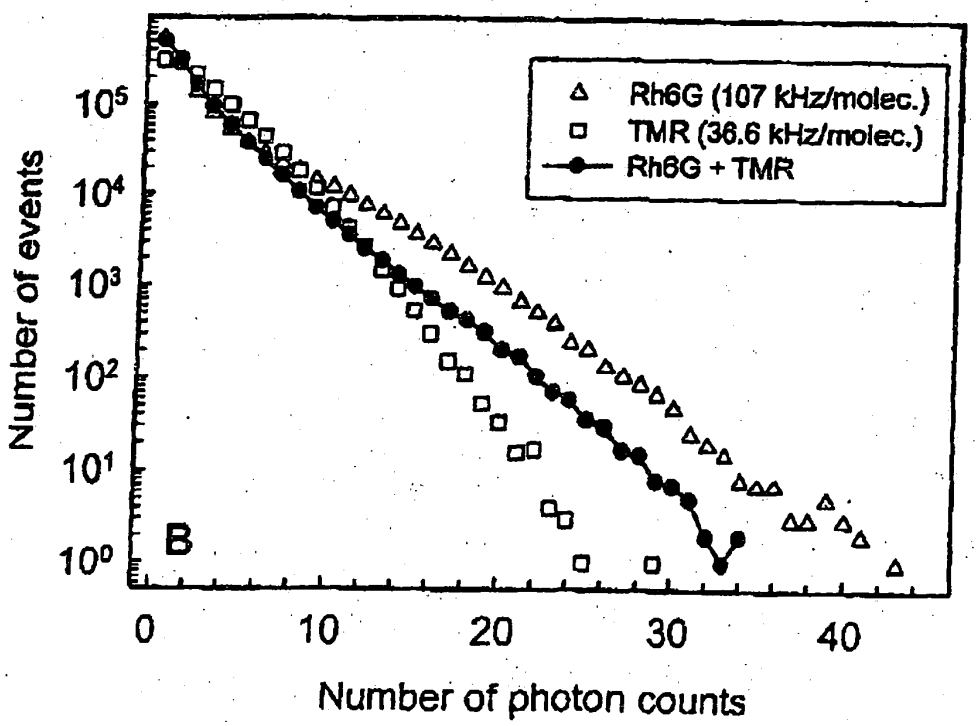
Number of events
Number of photon counts
B
Rh6G (107 kHz/molec.)
TMR (36.6 kHz/molec.)
Rh6G + TMR

Fig. 10 A,B

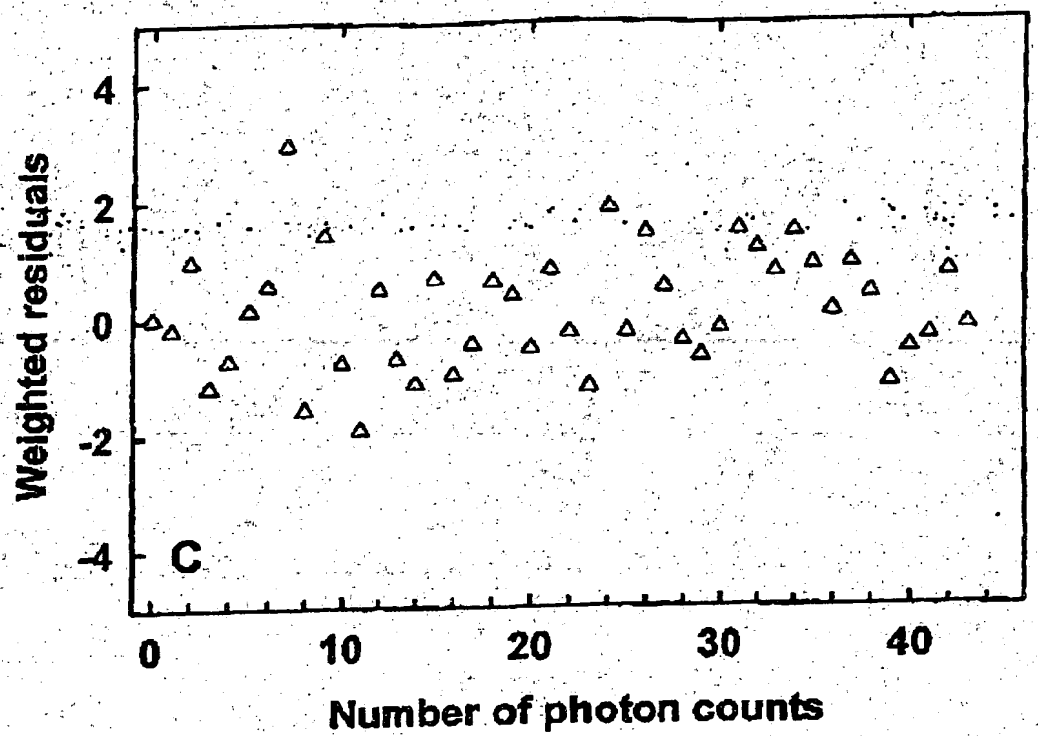
Weighted residuals
4
2
0
-2
-4
C
0
10
20
30
40
Number of photon counts

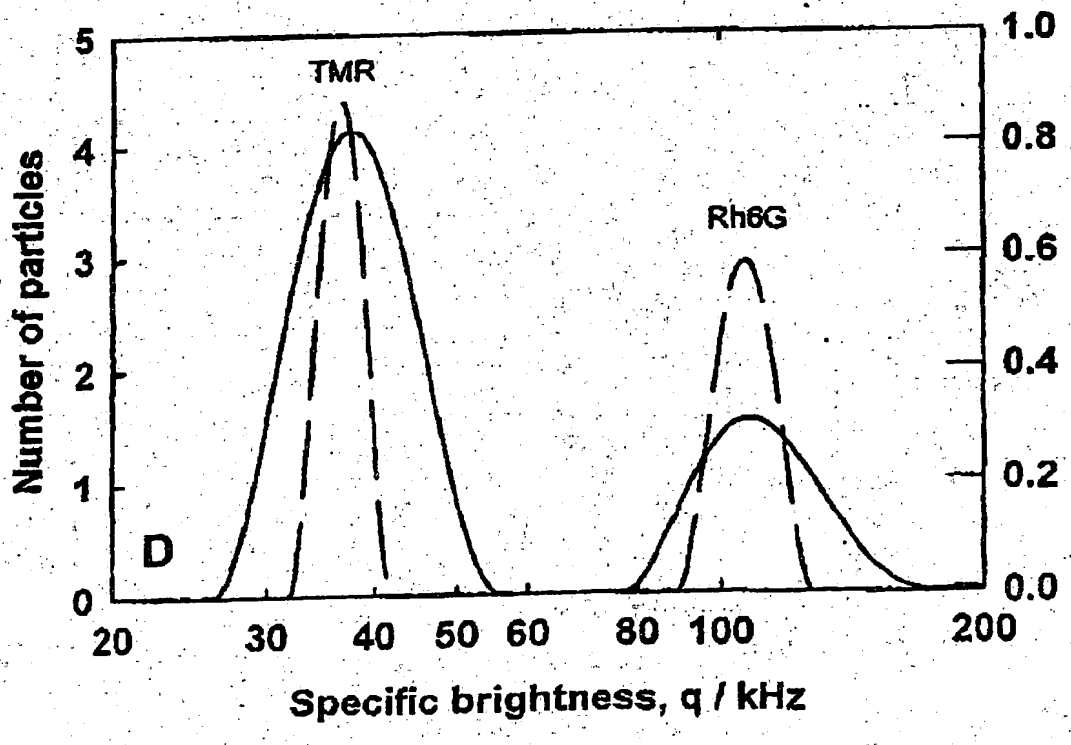
TMR
Rh6G
Number of particles
5
4
3
2
1
0
D
1.0
0.8
0.6
0.4
0.2
0.0
20
30
40
50
60
80
100
200
Specific brightness, q / kHz

Fig. 10 C,D

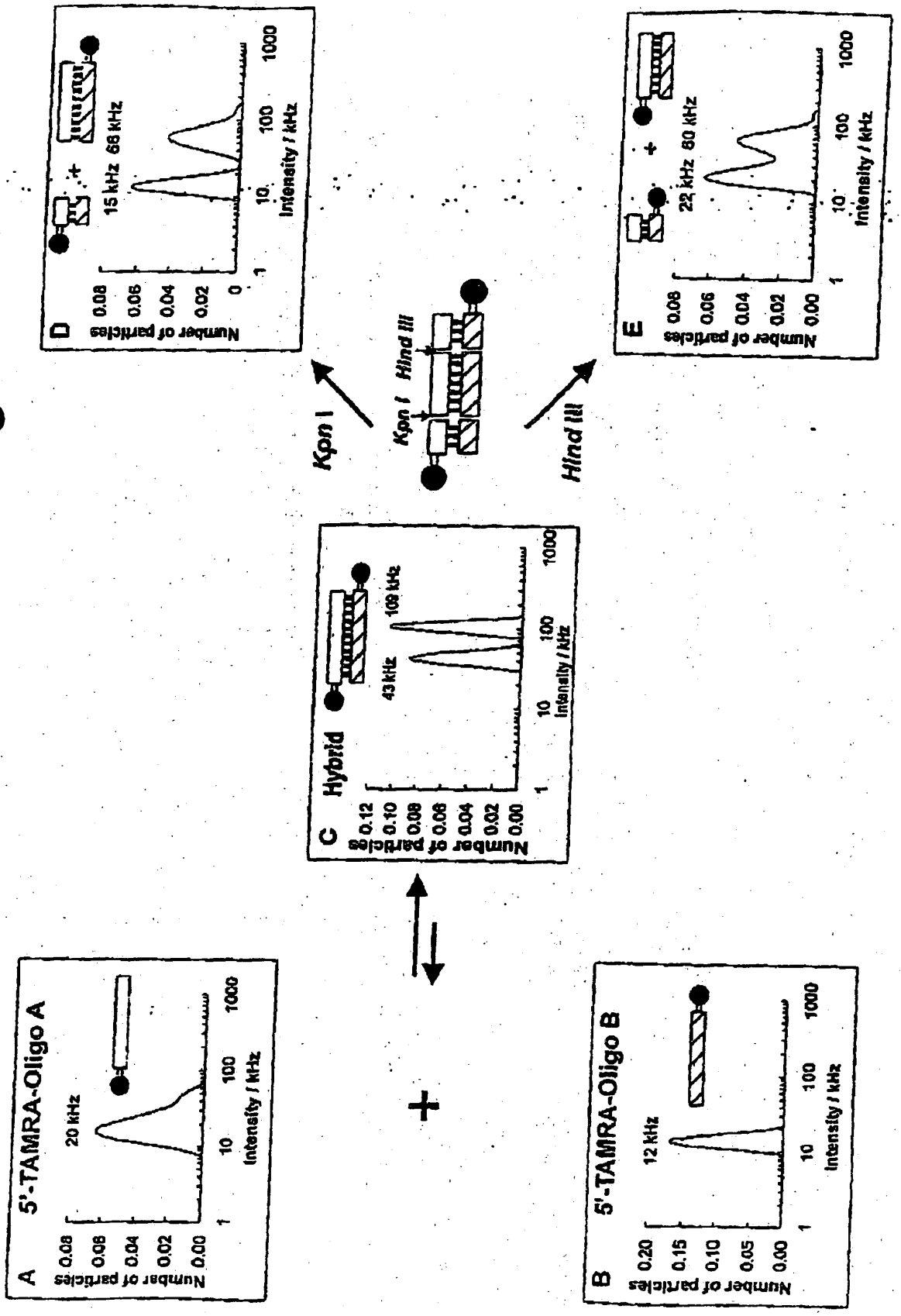
A
5'-TAMRA-Oligo A
20 kHz
Number of particles
Intensity / kHz
B
5'-TAMRA-Oligo B
12 kHz
Number of particles
Intensity / kHz
C
Hybrid
43 kHz
109 kHz
Number of particles
Intensity / kHz
D
15 kHz
68 kHz
Number of particles
Intensity / kHz
E
22 kHz
80 kHz
Number of particles
Intensity / kHz
Kpn I
Hind III
Kpn I
Hind III

Fig. 11

B

Cleavage	Intensity / kHz		
none	Q_{01} = 43/109 (48/52)*	Q_{02} = 16/60 (9/91)*	Q_{03} = 25/66 (12/88)*
Hind III	Q_1 = 60 Q_3 = 22	Q_1 = 58	Q_3 = 26
Kpn I	Q_3 = 15 Q_4 = 66	Q_3 = 12	Q_4 = 80
Hind III/*Kpn* I	Q_3 = 24 Q_3 = 10	Q_3 = 12	Q_2 = 28

*Concentration ratio (%) of two signals. See text for details.

Fig. 12

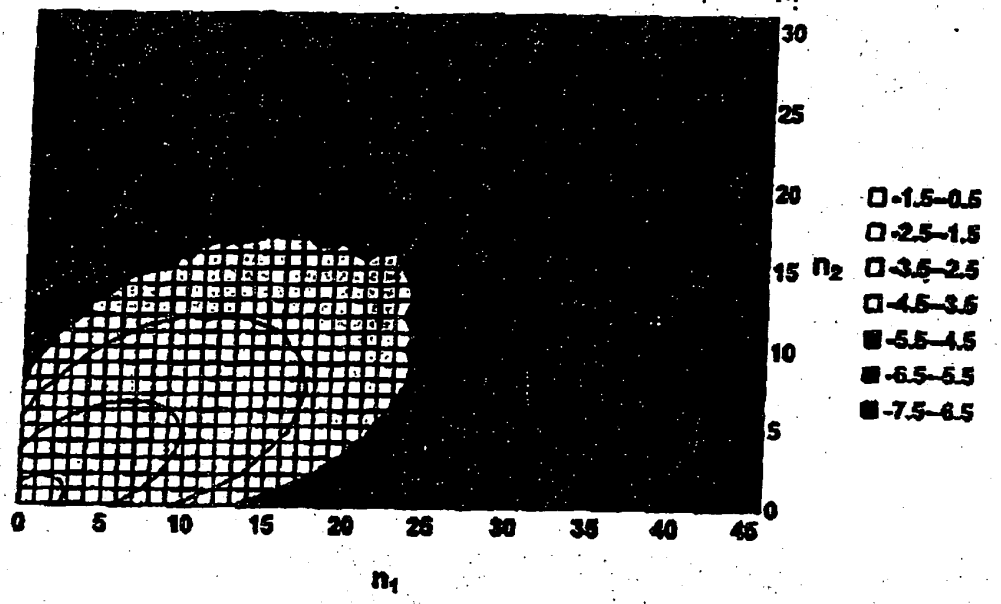
30
25
20
15
10
5
0
n_2
0 5 10 15 20 25 30 35 40 45
n_1
-1.5–0.5
-2.5–1.5
-3.5–2.5
-4.5–3.5
-5.5–4.5
-6.5–5.5
-7.5–6.5

Fig. 13

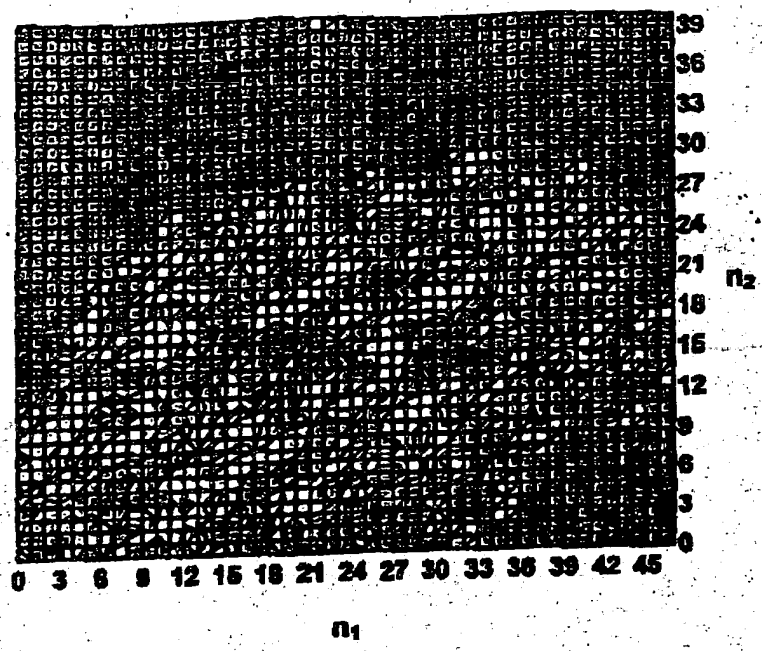
39
36
33
30
27
24
21
18
15
12
9
6
3
0
n_2
0 3 6 9 12 15 18 21 24 27 30 33 36 39 42 45
n_1

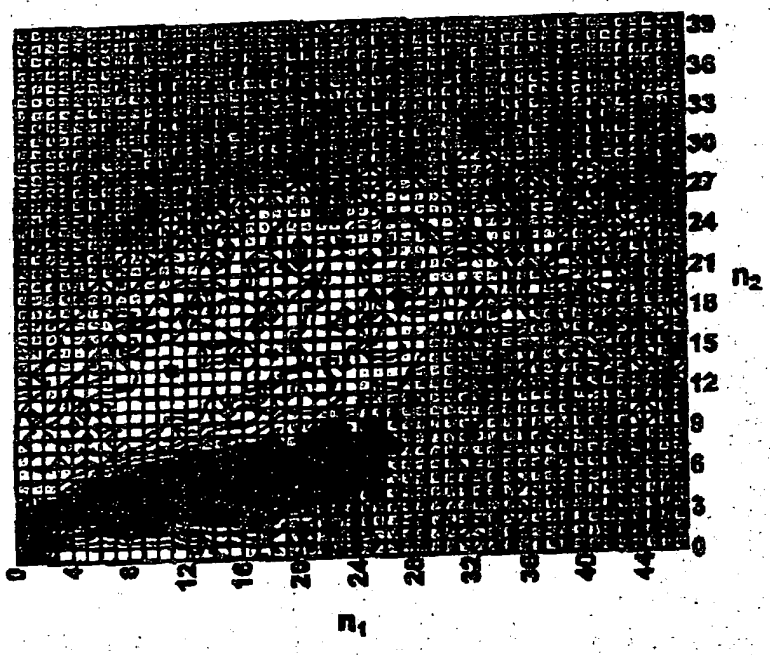
39
36
33
30
27
24
21
18
15
12
9
6
3
0
n_2
0 4 8 12 16 20 24 28 32 36 40 44
n_1
6-8
4-6
2-4
0-2
-2-0
-4--2
-6--4
-8--6

Fig. 14

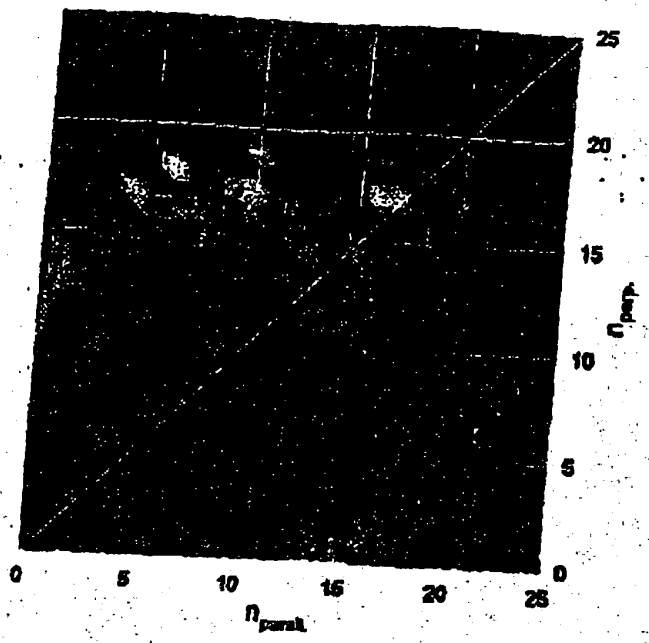
25
20
15
10
5
0
0
5
10
15
20
25
$n_{perp.}$
$n_{paral.}$

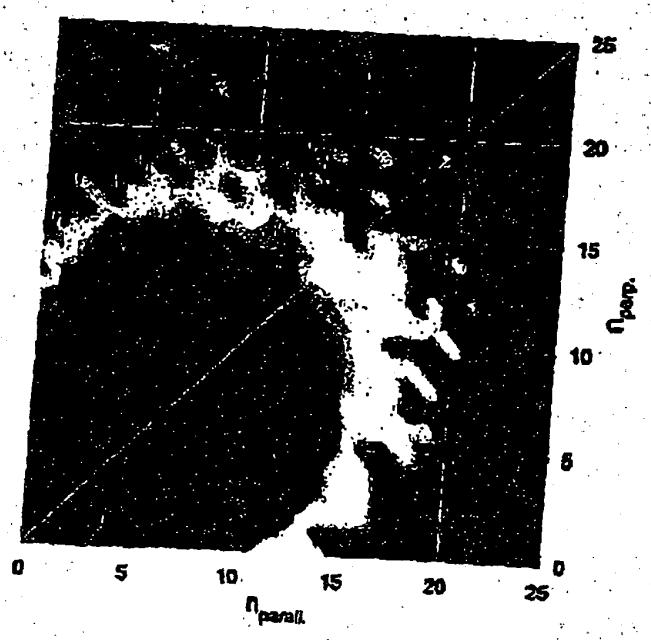
25
20
15
10
5
0
0
5
10
15
20
25
$n_{perp.}$
$n_{paral.}$

Fig. 15

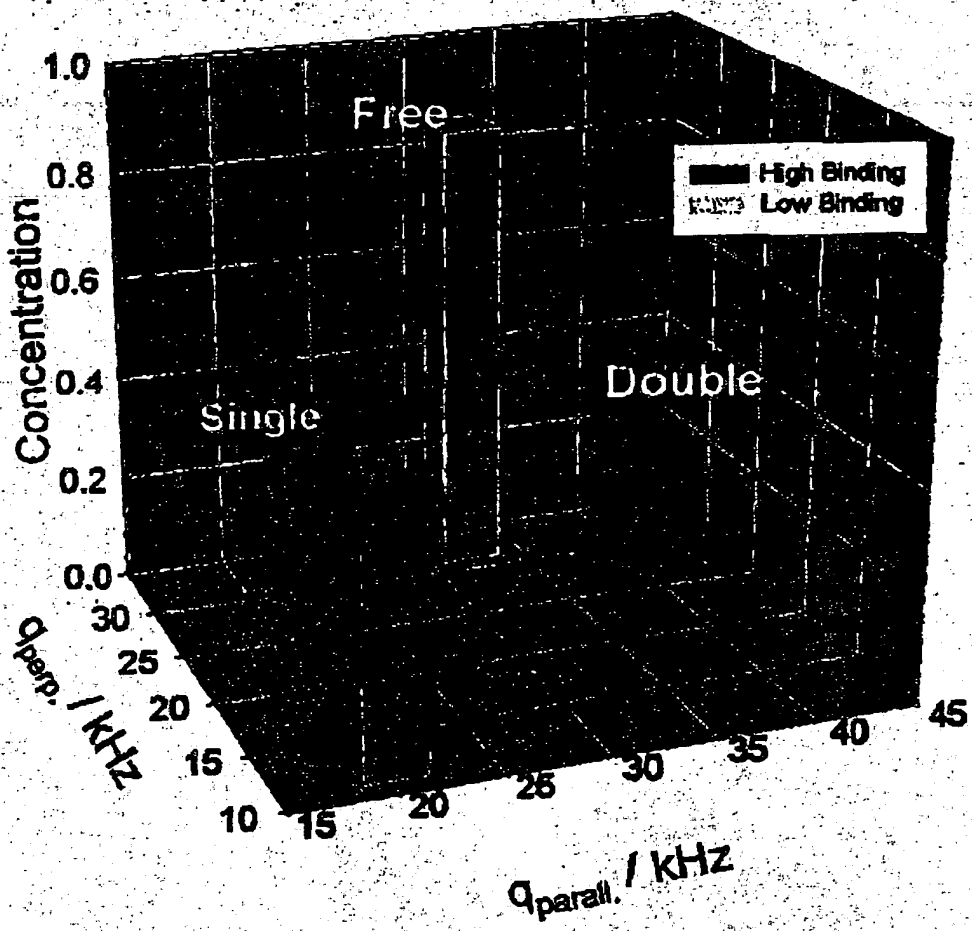
Free
High Binding
Low Binding
Single
Double
Concentration
1.0
0.8
0.6
0.4
0.2
0.0
q perp. / kHz
30
25
20
15
10
15
20
25
30
35
40
45
q parall. / kHz

Fig. 16

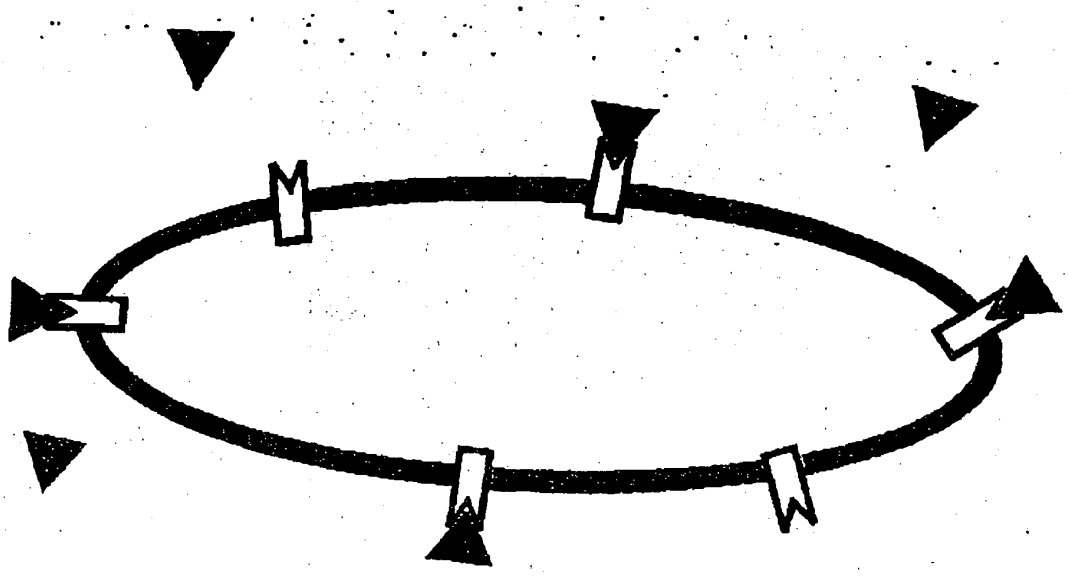

Fig. 17

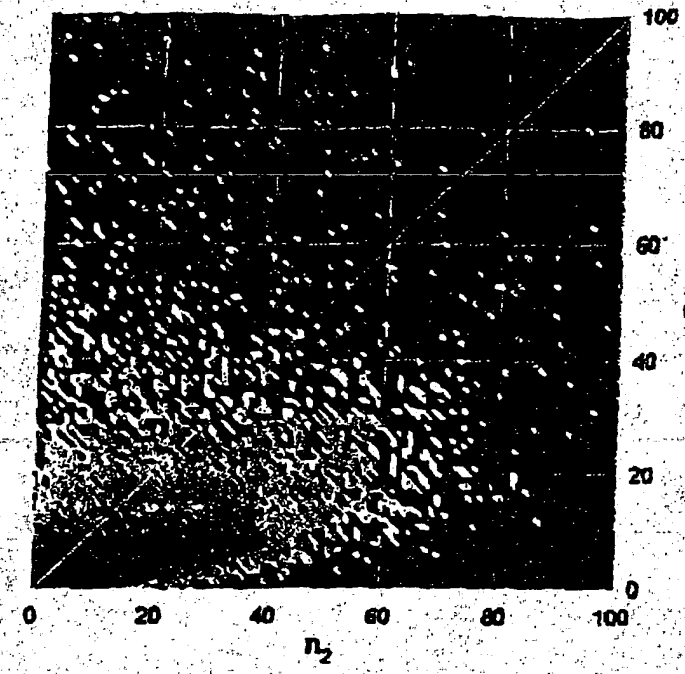
100
80
60
40
20
0
n_1
0
20
40
60
80
100
n_2

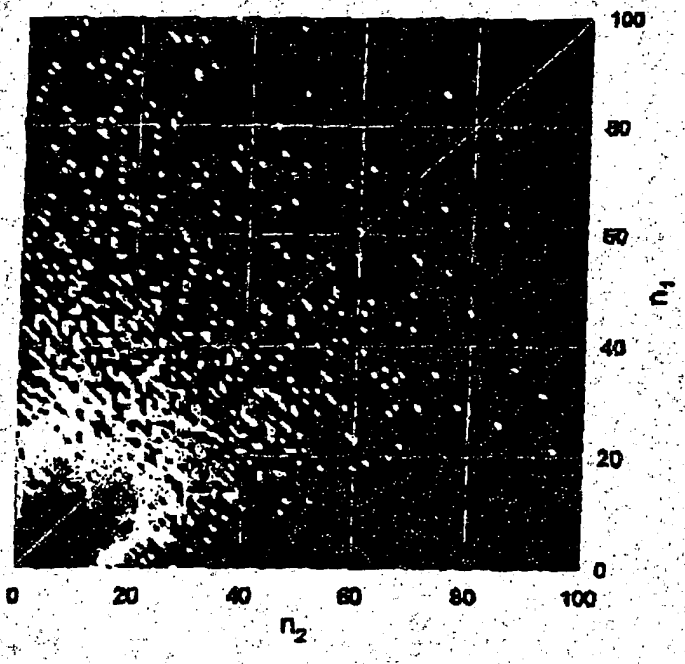
100
80
60
40
20
0
n_1
0
20
40
60
80
100
n_2

Fig. 18

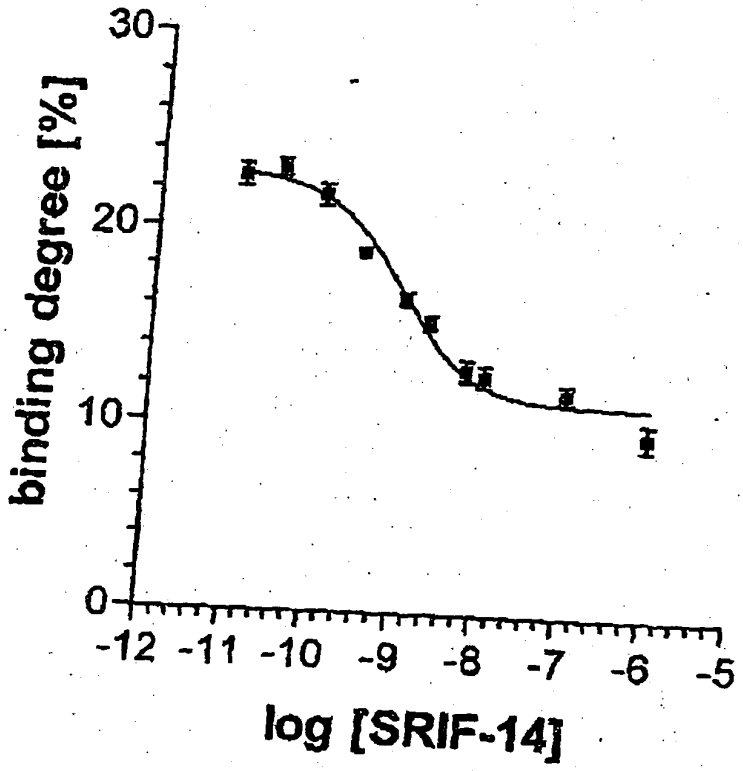

Fig. 19

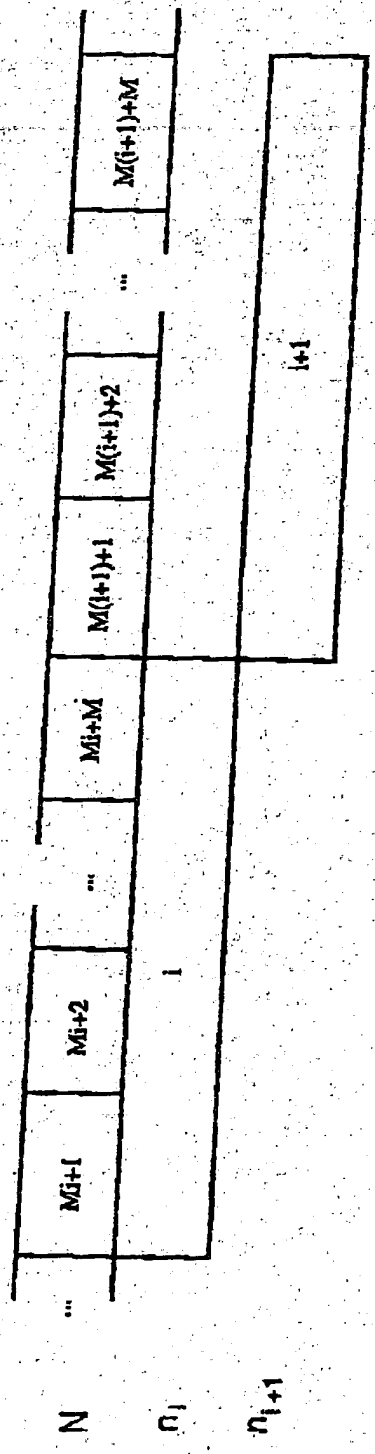

Fig. 20

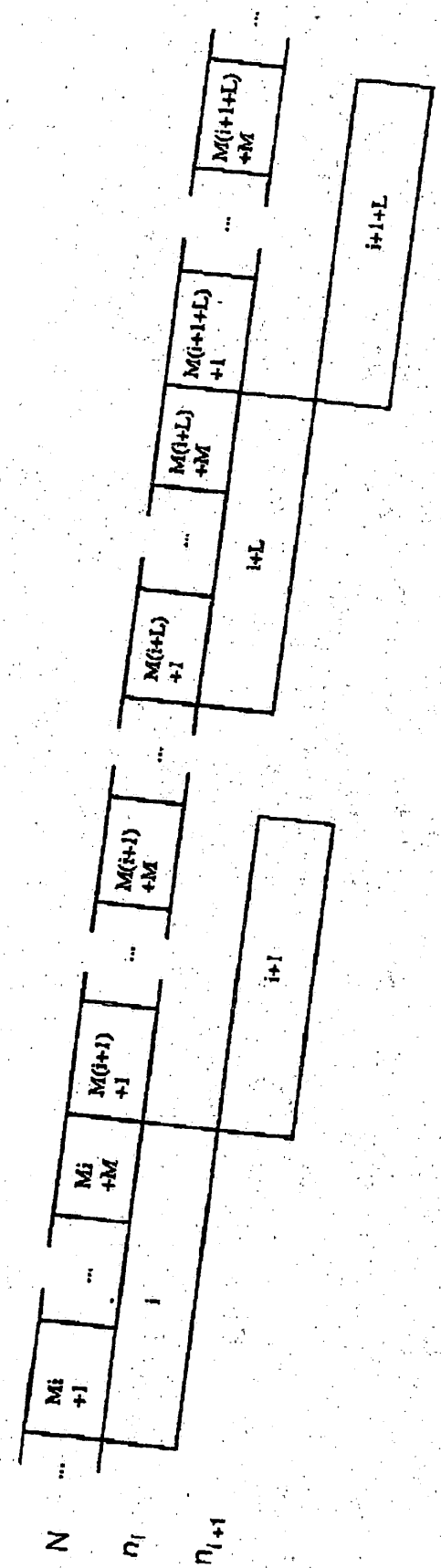

Fig. 21

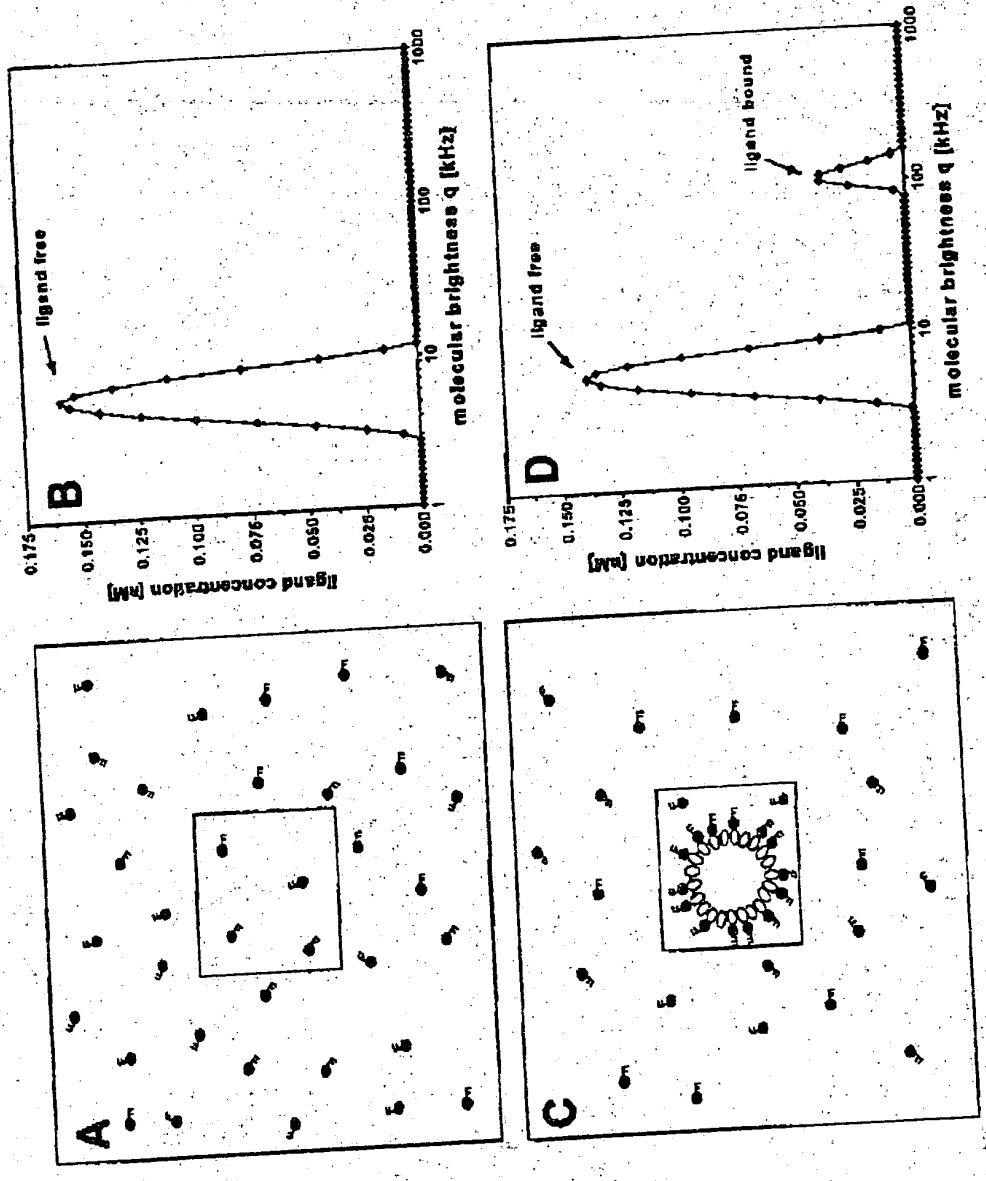
A
B
C
D
ligand free
ligand bound
molecular brightness q [kHz]
ligand concentration [nM]
0.175
0.150
0.125
0.100
0.075
0.050
0.025
0.000
1000
100
10
1

Fig. 22

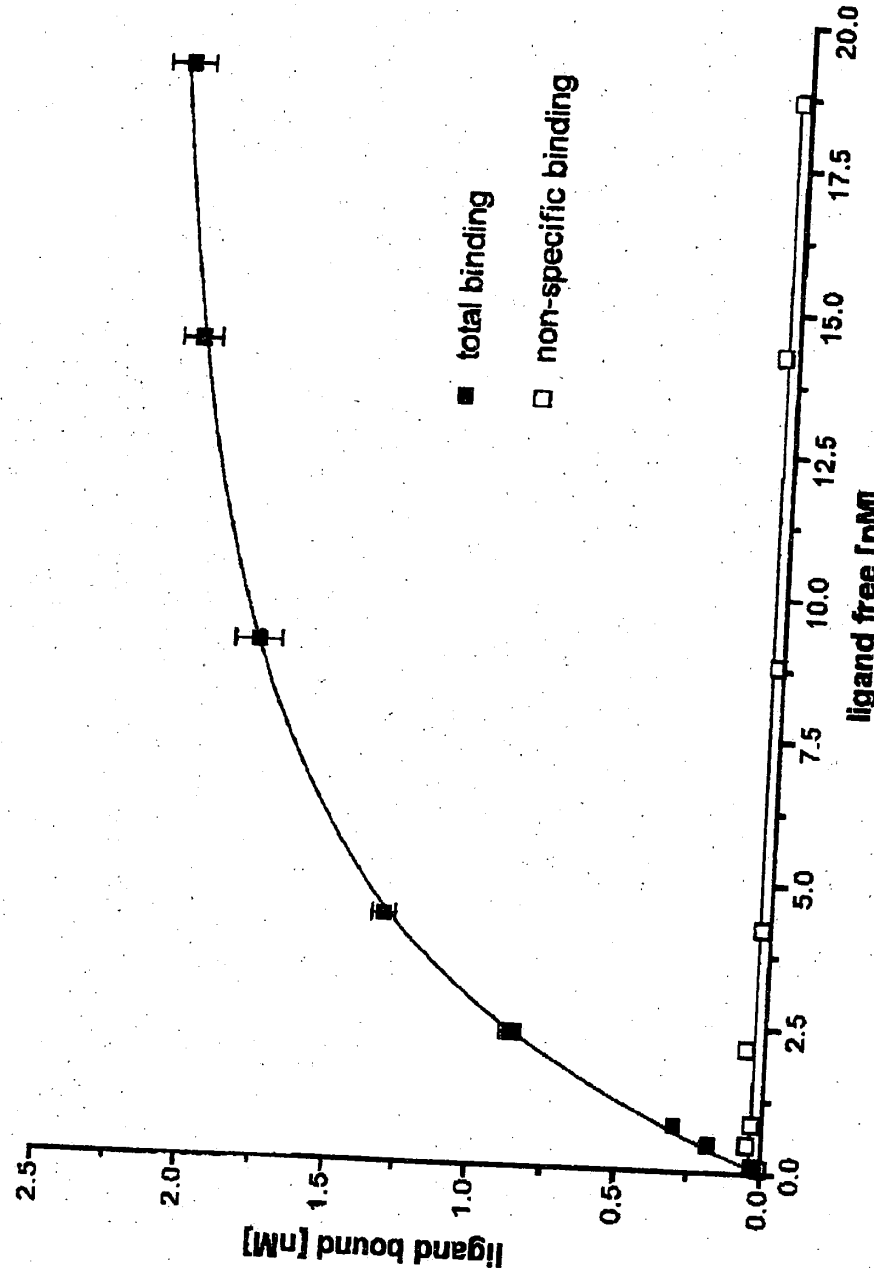
total binding
non-specific binding
ligand bound [nM]
ligand free [nM]
0.0
0.5
1.0
1.5
2.0
2.5
0.0
2.5
5.0
7.5
10.0
12.5
15.0
17.5
20.0

Fig. 23

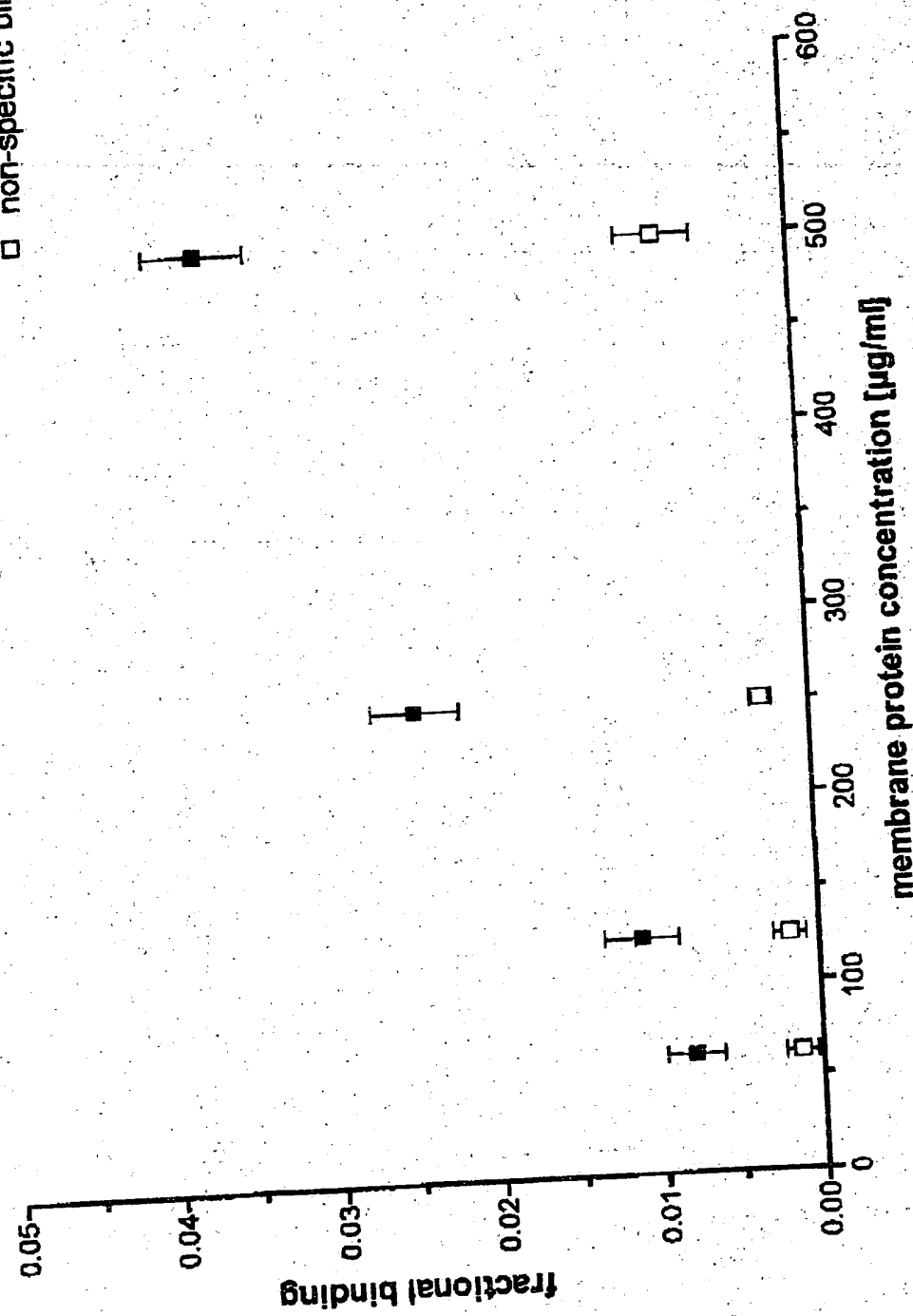
total binding
non-specific binding
fractional binding
0.00
0.01
0.02
0.03
0.04
0.05
membrane protein concentration [µg/ml]
0
100
200
300
400
500
600

Fig. 24

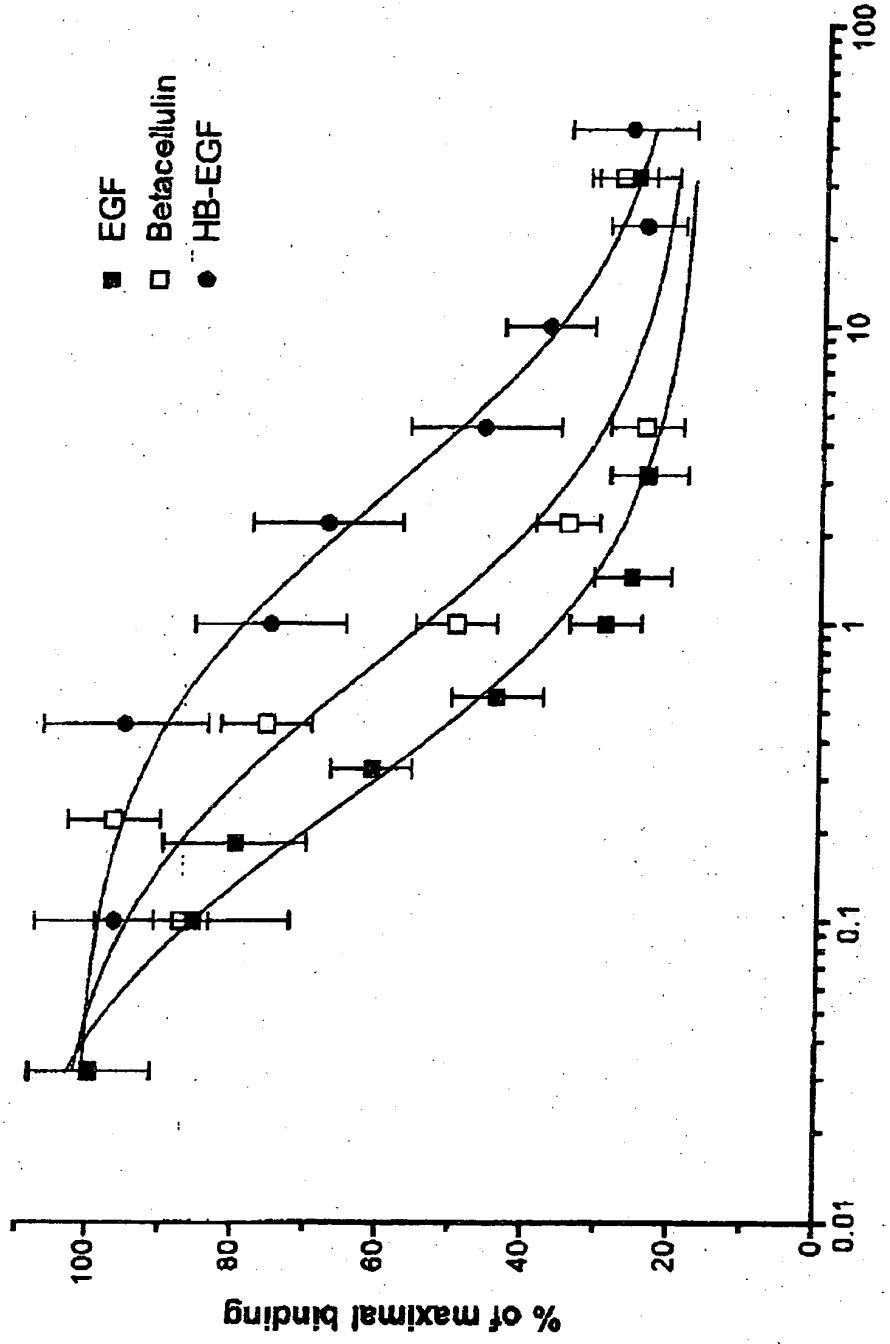
EGF
Betacellulin
HB-EGF
% of maximal binding
competitor [nM]
0
20
40
60
80
100
0.01
0.1
1
10
100

Fig. 25

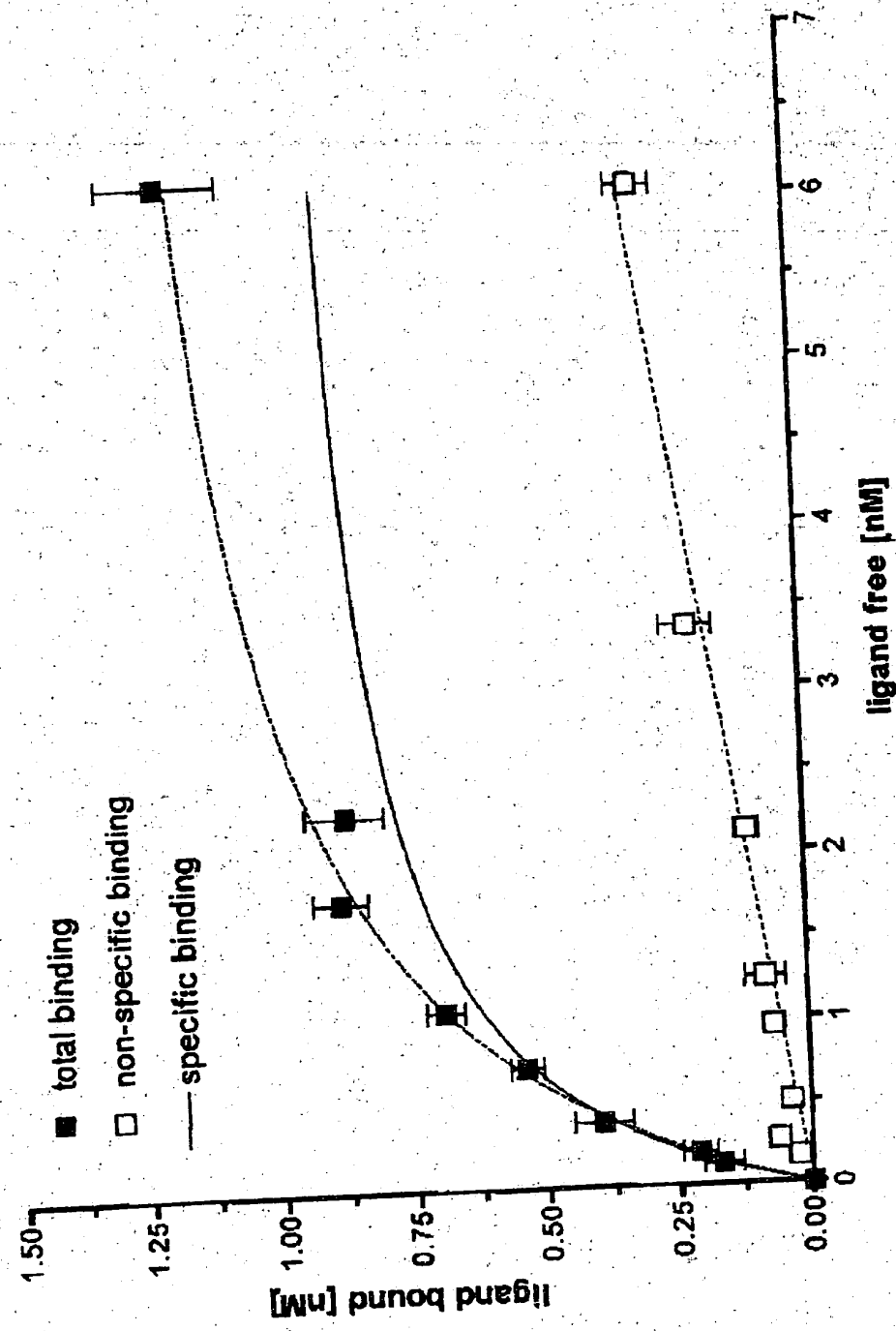
total binding
non-specific binding
specific binding
ligand bound [nM]
1.50
1.25
1.00
0.75
0.50
0.25
0.00
ligand free [nM]
0
1
2
3
4
5
6
7

Fig. 26

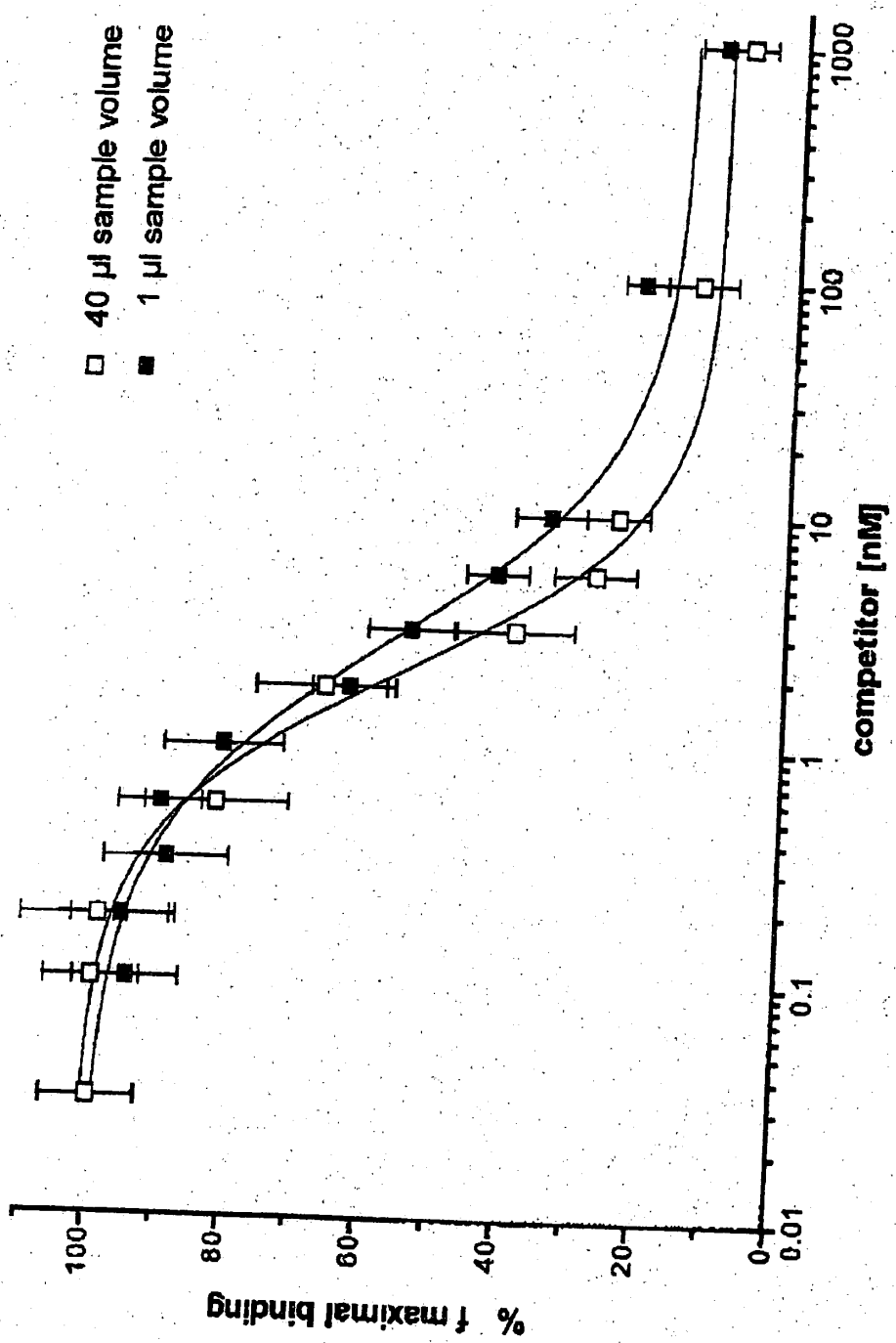
40 µl sample volume
1 µl sample volume
% f maximal binding
100
80
60
40
20
0
0.01
0.1
1
10
100
1000
competitor [nM]

Fig. 27

29/29